

The Role of Fluid Dynamics, Microstructure and Mucociliary Clearance in the Micro- and Macroscopic Barrier Properties of Pulmonary Mucus

Dissertation

zur Erlangung des Grades

des Doktors der Naturwissenschaften

der Naturwissenschaftlich-Technischen Fakultät III

Chemie, Pharmazie, Bio- und Werkstoffwissenschaften

der Universität des Saarlandes

von

Julian Kirch

Saarbrücken

2012

Tag des Kolloquiums:	31. Oktober 2012
Dekan:	Prof. Dr. Wilhelm F. Maier
Vorsitzender:	Prof. Dr. R.W. Hartmann
Berichterstatte r:	Prof. Dr. C.-M. Lehr
	Prof. Dr. I. Bernhardt
	Prof. Dr. B. Rothen-Rutishauser
Wissenschaftlicher Mitarbeiter:	Dr. G.-W. Kohring

Für meine Frau Sabrina

“Reality is frequently inaccurate.”

The Hitchhikers Guide to the Galaxy, Douglas Adams

Table of Contents

1. Summary	- 1 -
2. Zusammenfassung	- 2 -
3. Introduction	- 3 -
3.1 Pulmonary Drug Delivery and Nanocarriers	- 4 -
3.2 Mucus and Mucociliary Clearance	- 7 -
3.3 Particle Mobility in Mucus and Hydrogels	- 11 -
3.4 Aim of This Work	- 15 -
4. Mucociliary Clearance of Nanoparticles	- 17 -
4.1 Abstract	- 18 -
4.2 Introduction	- 18 -
4.3 Experimental	- 20 -
4.3.1 Materials	- 20 -
4.3.2 Particle Tracking Experiments	- 21 -
4.3.3 Particle Characterization	- 23 -
4.4 Results	- 24 -
4.4.1 Particle Characterization	- 24 -
4.4.2 Particle Tracking Experiments	- 26 -
4.5 Discussion	- 28 -
4.6 Conclusion	- 31 -
5. Fluid Dynamics of Particle-Mucus Interactions	- 32 -
5.1 Abstract	- 33 -
5.2 Introduction	- 33 -
5.3 Experimental	- 35 -
5.3.1 CFD and Analytical Solution of Particle Trajectories	- 35 -
5.3.2 Simulation of Mucus Plasticity	- 38 -
5.4 Results	- 39 -
5.4.1 Particle Trajectories	- 39 -
5.4.2 Simulation of Mucus Plasticity	- 44 -
5.5 Discussion	- 45 -
5.5.1 Particle Trajectories	- 45 -

5.5.2	<i>Mucus Plasticity</i>	- 46 -
5.6	Conclusion	- 47 -
6.	The Role of Micro- and Macrostructure of Mucus in Particle Mobility	- 48 -
6.1	Abstract	- 49 -
6.2	Introduction	- 49 -
6.3	Experimental	- 51 -
6.3.1	<i>Materials</i>	- 51 -
6.3.2	<i>Atomic Force Microscopy</i>	- 52 -
6.3.3	<i>Capillary Penetration Experiments</i>	- 54 -
6.3.4	<i>Cryo-SEM</i>	- 55 -
6.3.5	<i>Optical Tweezers</i>	- 55 -
6.4	Results	- 59 -
6.4.1	<i>Force Spectroscopy</i>	- 59 -
6.4.2	<i>Capillary Experiments</i>	- 59 -
6.4.3	<i>Cryo-SEM</i>	- 62 -
6.4.4	<i>Optical Tweezers</i>	- 64 -
6.5	Discussion	- 69 -
6.5.1	<i>Force Spectroscopy</i>	- 69 -
6.5.2	<i>Capillary Experiments</i>	- 69 -
6.5.3	<i>Cryo-SEM</i>	- 70 -
6.5.4	<i>Optical Tweezers</i>	- 71 -
6.6	Conclusion	- 73 -
7.	Overall Conclusion and Outlook	- 74 -
8.	List of Figures	- 77 -
9.	List of Abbreviations	- 78 -
	References	- 79 -
	Curriculum Vitae	- 89 -
	List of Publications	- 91 -
	Scientific Publications	- 91 -
	Poster & Talks	- 92 -
	Acknowledgements	- 94 -

1. Summary

Major issues in both toxicological as well as pharmaceutical research are biological barriers, impeding the invasion of pathogens but also the delivery of beneficial substances into the body. The upper lungs as site of application of such substances exhibit a particularly efficient biological barrier: the mucus blanket and its mucociliary clearance. The fate of particles upon deposition onto the moving mucus barrier is yet unsolved and was central theme of this work. In this context, mucociliary clearance of nanoparticles and its fluid dynamics were investigated. These results were correlated with the analysis of microscopic and macroscopic particle penetration behavior in mucus and mucus structure. Here, the application of complex methods such as cryoscopic scanning electron microscopy (cryo-SEM), atomic force microscopy (AFM) and optical tweezers revealed the mechanisms of particle mobility in mucus. It could be shown that mucociliary clearance is independent on particle properties such as size, shape, charge or surface chemistry. It was demonstrated that this is due to the only poor particle mobility in mucus: The polymer scaffold of mucus is highly rigid which, in combination with the extensive heterogeneity in pore size, impedes particle translocation. In contrast to model gels and due to this rigidity, particles in mucus which are exposed to external force fields cannot deform or rupture the polymer scaffold of mucus.

2. Zusammenfassung

Ein zentrales Thema sowohl in der toxikologischen als auch der pharmazeutischen Forschung sind biologische Barrieren, welche die Aufnahme von Krankheitserregern aber auch Pharmazeutika in den Körper erschweren. Die obere Lunge als Applikationsort solcher Substanzen weist eine besonders effiziente biologische Barriere auf: die Mukus-Schicht mit ihrer mukoziliären Clearance. Das Schicksal von Partikeln nach deren Deposition auf der bewegten Mukus-Schicht ist noch ungeklärt und war zentrales Thema dieser Arbeit. In diesem Kontext wurde die mukoziliäre Clearance von Nanopartikeln und deren Fluid Dynamik untersucht. Die Ergebnisse wurden mit der Analyse des mikro- und makroskopischen Penetrationsverhaltens von Partikeln in Mukus und dessen Struktur korreliert. Dabei deckte die Anwendung von Kryo-Elektronenmikroskopie, Rasterkraftmikroskopie und der optischen Pinzette die Mechanismen der Partikelmobilität in Mukus auf. Zusammenfassend konnte gezeigt werden, dass die mukoziliäre Clearance unabhängig von Partikelgröße, -form, -ladung, oder -oberflächenchemie ist. Es wurde nachgewiesen, dass dies auf die vernachlässigbare Partikelmobilität in Mukus zurückzuführen ist: Das Polymergerüst von Mukus ist hoch rigide, was aufgrund der großen Heterogenität der Porengröße die Partikeltranslokation behindert. Im Gegensatz zu den verwendeten Modell-Gelen und aufgrund dieser Rigidität können Partikel, die einem externen Kraftfeld ausgesetzt sind, das Polymergerüst von Mukus nicht zerstören.

3. Introduction

3.1 Pulmonary Drug Delivery and Nanocarriers

The pulmonary route to deliver drugs is one of the earliest forms of drug administration to treat diseases (Bailey and Berkland, 2009). Not considering the use of “vapors” by Egyptians in 1500 B.C., such applications even date as early as the late 17th century when Bennet used inhalation treatments to cure tuberculosis (Patton and Byron, 2007). With growing technological knowledge, inhalation made its way into the 20th century and became a convenient and effective treatment in various therapies. By now, inhalation of drugs as droplet aerosol or dry powder is used not only in local but also systemic applications. While the former has played a more important role in the beginning of inhalation therapy (asthma, tuberculosis and obstructive disorders), the latter is already being exploited in various diseases (e.g. insulin delivery) with more applications still to come. The advantages of pulmonary delivery, grasped only empirically in the beginning, are now being widely appreciated in particular with respect to the delivery of modern formulations: Crucial for any type of drug delivery application is the performance in uptake/absorption, stability and retention, i.e. the (time dependent) concentration in the blood of the delivered active pharmaceutical ingredient (API) in comparison to intravenous application which can be summarized by the term “bioavailability”. Not only in this respect, the pulmonary route holds great potential: The large surface area, high epithelial permeability and low catabolic enzymatic activity allow for rapid and effective uptake of drugs. In addition, it has the specific advantage of avoiding first-pass effects and potential side-effects of high systemic concentrations typical of conventional delivery methods (Bailey and Berkland, 2009). Furthermore, the convenience and adherence of such a form of delivery versus oral dosage forms or even injections are highly relevant in clinical practice or pediatrics. Especially with respect to therapies or vaccination in third world countries, where injections pose a major risk to infections, this aspect is particularly important.

In the past, the focus of research in aerosol medicine has been laid on the optimization of drug carrier deposition in the lungs. Here, implications of physical and aerodynamic properties of such carriers and of the design of inhalation devices on the deposited particle or droplet fraction had to be thoroughly understood to control deposition in the desired way. Especially particle size distribution and the respective size-associated deposition mechanisms (impaction, sedimentation and diffusion) were extensively investigated: In

particular in terms of systemic delivery, it is often desired to deposit particles in the deeper lungs where the large surface area and thin epithelium enhance drug uptake. To advance this deep into the lungs, the aerosol needs a certain particle/droplet size distribution to avoid deposition or impaction in the upper parts of the lungs. Particles with aerodynamic diameters of approximately 1-5 μm are considered ideal for alveolar deposition (Scheuch, Kohlhaeufel et al., 2006). Above and below this size, particles or droplets are preferably deposited in the trachea or bronchia (figure 1). However, new technologies such as larger carriers doped with nanoparticles which can be released after deposition are applied to overcome these aerodynamic restriction. Thus, it is possible to combine existing knowledge of optimal aerosolization and thus deposition patterns with the advantages of the more recent concept of nanocarriers. In current opinion, these nanoparticles are objects with at least one dimension $< 100 \text{ nm}$ (Oberdorster, Oberdorster et al., 2005) while in the pharmaceutical context, this is often extended to particulate matter of several hundred nanometers in size (Kreuter, 1991).

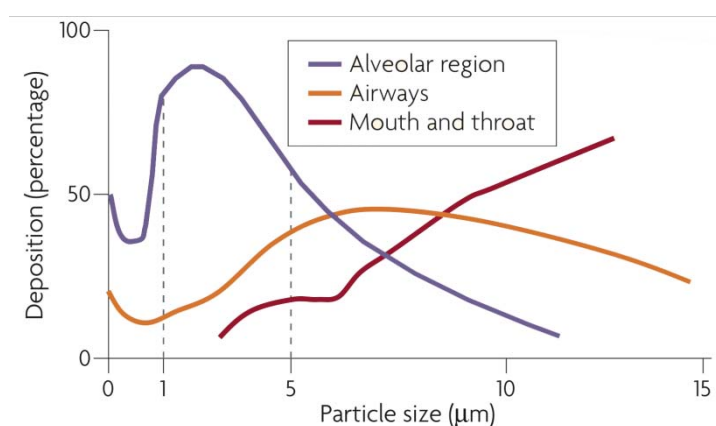


Figure 1: Particle deposition in dependency of particle size (aerodynamic diameter). Particles of an aerodynamic diameter between 1 and 5 μm are considered ideal for alveolar deposition whereas smaller and larger particles are preferably deposited in the airways or the mouth and throat, respectively. By courtesy of Christian Ruge, adopted from (Patton and Byron, 2007).

One key feature of these benefits of the application of nanoparticles is linked with the mentioned term of bioavailability: In current research, the development of new applications for systemic delivery, mostly involving fragile and costly (macro)molecules or proteins, demands more than an optimal particle or droplet deposition as stability and

delivered amount are much more restricted than in conventional drugs. Therefore, in this case, an optimization of dissolution properties, stability and targeting is enormously more important. These factors can be positively influenced by the use of nanocarriers. The small size and thus the surface area of these particles greatly improves dissolution behavior even without the use of enhancers with often unknown long-term safety (Bailey and Berkland, 2009). Furthermore, it is widely accepted that smaller particles ($< 0.5 \mu\text{m}$) may be taken up in a more effective way by cells than larger particles (Koch, Reynolds et al., 2005; Bailey and Berkland, 2009). This may be the reason that nanoparticles exhibit prolonged retention compared to microparticles (Geiser and Kreyling, 2010). These uptake properties also provide the potential to improve the targeting to specific cell types or intracellular compartments.

One big issue in the characterization of the potential of nanocarriers in terms of bioavailability refers to the aspects of retention and penetration. Retention describes the performance of a formulation in resisting the respective forms of clearance characteristic for the site of delivery. For intravenous delivery the prominent forms are typically the renal and hepatic clearance. In pulmonary delivery, however, this refers mainly to the mucociliary- and the macrophage clearance. Mucociliary clearance is the dominant form of clearance in the central and upper lungs whereas macrophage clearance is more dominant in the alveoli. Penetration is important, as the thick mucus layer in the upper lungs (figure 2) is not only excreting deposited particles by mucociliary clearance but forms a compact non-epithelial barrier which nanocarriers have to cross before reaching the epithelium or even the blood stream. The work presented here, focuses on the local pulmonary delivery in the upper lungs as it is relevant for diseases such as chronic obstructive pulmonary disease (COPD) or pulmonary hypertension where frequent and long-lasting local treatment is necessary. Here, the need for modern formulations with sustained, local release, and thus a minimized drug or carrier clearance, is paramount. Therefore, mucociliary clearance and mucus penetration which have been under investigation for quite some time but are not sufficiently understood so far, are very important in this field, particularly for nanoparticle delivery. Here several mechanisms are exclusive for such small carriers (e.g. wetting phenomena and fluid dynamics) and have to be thoroughly considered to evaluate the pharmaceutical potential of the carrier.

3.2 Mucus and Mucociliary Clearance

Mucociliary clearance is an innate airway defense mechanism enabling the body to excrete foreign material in a very efficient way. The underlying principle is the constant secretion of mucus and its fast cranial propulsion (3-25 mm/min in humans (Hofmann and Asgharian, 2003; Antunes and Cohen, 2007)) by the concerted action of beating cilia attached to the tips of the epithelial cells (figure 2). Thus, airborne pathogens, dust or other foreign material can be trapped inside the mucus layer and removed from the airways. Mucus is a complex fluid consisting of proteins, electrolytes and water. As biological hydrogel, the water content is very high (95 % by weight). The macromolecular hydrogel structure is given by mucins (< 5 % by weight). The remaining components are inorganic salts, carbohydrates and lipids (Peppas and Huang, 2004). Mucins are large proteins containing highly hydrophilic glycosylated regions as well as “naked” and thus more hydrophobic domains. The sugar content usually represents up to 50 % of the protein weight where the sugar chains are attached via O-glycosidic bounds between N-acetylgalactosamine and serine or threonine residues (Sanders, Rudolph et al., 2009); further sugar residues are galactose, fucose and sialic acids. The dominating amino acids in the protein backbone are serine, threonine and proline (Peppas and Huang, 2004). The typical monomer length is 500 nm with a weight of 2-16 MDa (Sanders, Rudolph et al., 2009). Each mucosal surface has its own characteristic mucin composition: in pulmonary mucus, MUC5AC and MUC5B are the most abundant mucins (Thornton and Sheehan, 2004).

The hydrogel structure of mucus is given by polymerization of these mucin monomers to form block copolymers. Here, mucin monomers are linked by disulfide bridges, physical entanglement or hydrophobic interactions between non-glycosylated domains (Thornton and Sheehan, 2004; Cone, 2009). The underlying principles of mucin polymerization, especially with regard to the formation of the complex structure of the different layers of the pulmonary mucosa remain yet unsolved. One of the more established models for the formation of the mucin hydrogel is the so called “jack-in-the-box” model, describing the formation of the gel by quick hydration of the mucins upon secretion in a condensed and non- or only less hydrated form (Verdugo, Deyrup-Olsen et al., 1987; Verdugo, 1991).

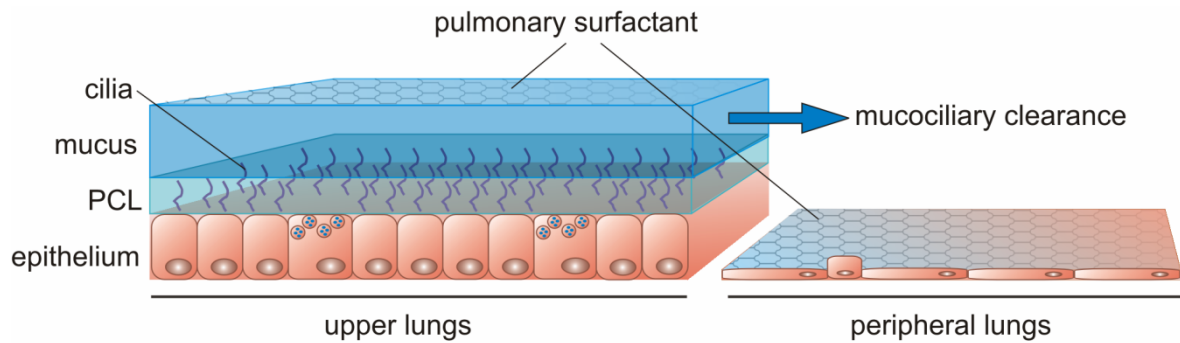


Figure 2: The lungs are lined with different non-epithelial barriers. In the peripheral lungs, the epithelium is lined with a very thin layer of surfactant. In the upper lungs, the epithelium is additionally covered with a thick barrier composed of the periciliary layer (PCL) of low viscosity and the highly viscoelastic “tenacious” (Florey, 1962) mucus layer.

This mechanism is also believed to contribute to the formation of the distinct two layer structure of the pulmonary mucosa: The epithelium of the upper lungs is lined with cells bearing 50-200 cilia per cell (Antunes and Cohen, 2007) which beat in a coordinated way to transport the mucus layer resting on the tips of these cilia. The cilia itself are moving in a layer of different properties, the periciliary layer (PCL). The PCL is located beneath the mucus blanket and is thought to be established by a gradient in mucin concentration proportional to the distance from the epithelium. Recent findings support the hypothesis of the PCL being interfused with tethered mucins, giving it some internal structure (Randell and Boucher, 2006). These more or less distinct layers differ mainly in rheological properties. Whereas the several micron thick mucus layer (0.2-30 μm (Sims and Horne, 1997; Widdicombe, 2002; Sanders, Rudolph et al., 2009)) is a gel of quite high viscosity, the underlying PCL is of lesser viscosity, believed to thus enable efficient ciliary beating. This difference in rheology is considered to be due to complex interactions between hydration status regulated by ion transporters, a gradient in mucin concentration and adaptation to environmental factors and mechanical stress (Tarran, Trout et al., 2006; Button and Boucher, 2008). The height of the PCL of approximately 7 μm (Button and Boucher, 2008) is given by the length of the cilia and is a key factor in the investigation of diseases such as cystic fibrosis (CF) which is associated with a defect in ion transport pathways affecting the volume of the PCL, the efficient ciliary beating and thus an impaired mucociliary clearance, leading to increased bacterial invasion. The thin layer (on average 200 nm (Bastacky, Lee et al., 1995)) of pulmonary surfactant (mainly composed of

phospholipids and proteins) on top of the mucus blanket has its major function in the deeper lungs, where it is the only non-epithelial barrier and contributes to the structural stability of the alveoli and immunological homeostasis.

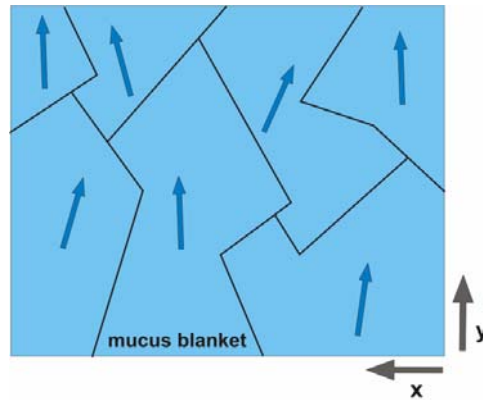


Figure 3: Metachronal fields describe areas of homogeneous mucus transport direction (blue arrows). The size of the field can differ over a large size range and is also different in healthy or diseased state (Iravani and Melville, 1976).

The beating pattern of the cilia is organized in so-called “metachronal fields” (Iravani and Melville, 1976) referring to the slight variance in space and time in the beating pattern of the cilia: The direction and the phase of the beating cycle (9-15 Hz in humans (Antunes and Cohen, 2007)) can be divergent in neighboring areas of the mucus blanket (figure 3). The areas of homogeneous transport direction and velocity are called metachronal fields.

While mucus clearance direction is heterogeneously organized in the horizontal (x - y) plane, other features of mucociliary clearance depend on the vertical position and thus the height above the epithelium. So far, the beating cycle of the cilia and the physical implications on mucus flow (fluid dynamics) are not completely solved. In the past years large efforts were focused on the mathematical modeling of the ciliary beating cycle (Barton and Raynor, 1967; Fulford and Blake, 1986; Smith, Gaffney et al., 2007), the complexity of the models and the results of this modeling approach clearly depending on the computing resources of the respective period. However, with only marginal experimental counterweight, these results show high variation, in particular for mucus flow

profiles, describing the velocity of the mucociliary transport in dependency of the height above the epithelium (Smith, Gaffney et al., 2008).

Similar to the (mathematical) description of the ciliary beating cycle, the interaction of particles with the mucus blanket and their mucociliary clearance has attracted much attention in the last years. Here, the focus was clearly laid on epidemiological or toxicological considerations, in particular with respect to pollution and exhaust, asbestos or the potential risk of exposure to newer materials such as carbon nanotubes. Therefore most of the data is acquired via scintigraphic or similar ensemble averaged methods, giving insight into the overall distribution or the cleared fraction of an inhaled particle species (Moller, Felten et al., 2008; Geiser and Kreyling, 2010). Parameters under investigation were particle size, shape and material, exposure and clearance time. Although it seems that there is consensus on the point that particle translocation through mucus and uptake into the blood stream is a minor clearance pathway compared to macrophage uptake and mucociliary clearance (Geiser and Kreyling, 2010), those studies do not give insight into the underlying mechanism of particle deposition onto and translocation within the mucus blanket on the single particle level. The investigation of the last point was previously assessed by microscopic methods to describe particle translocation phenomena *in vivo*. Here, large particles ($> 10 \mu\text{m}$) were observed to translocate into the pulmonary epithelium, which was concluded to be mainly due to wetting forces of the pulmonary surfactant (Schürch, Gehr et al., 1990; Gehr, Green et al., 1996). However, these results cannot be used to judge nanoparticle fate upon deposition onto the mucus blanket (figure 4).

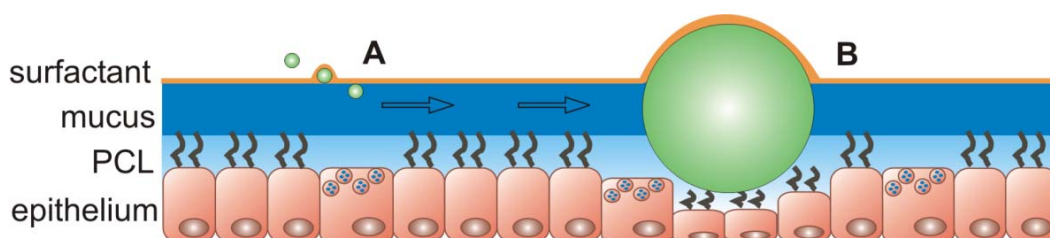


Figure 4: Particle translocation upon deposition onto the mucus blanket depends on size. Wetting forces can maximally submerge small particles completely but not cause further translocation through mucus (A). Particles with a diameter approaching the thickness of PCL and mucus, however, can be pushed inside the epithelium due to wetting forces (B).

In this case, wetting forces may cause a immersion of nanoparticles below the surface of the mucus blanket, but do not influence particle mobility inside mucus and thus do not cause a translocation through mucus towards the epithelium. This is particularly true if the fluid layer on top of the epithelium is several microns thick as it is in the upper lungs. Therefore, the fate of nanoparticle upon deposition onto mucus is not sufficiently solved yet and satisfying studies are still missing.

3.3 Particle Mobility in Mucus and Hydrogels

The non-epithelial barrier of the pulmonary mucus blanket in the upper lungs derives its barrier properties not only from the ciliary clearance and thus the fast excretion of inhaled material. As mentioned before, the highly viscous and compact mucus layer impedes translocation of pathogens or particulate matter to the epithelium. Similar to other hydrogels, hydrated mucins in mucus form a tight mesh of entangled fibers, trapping any material entering the mucus. In physical terms, this system can be described as complex fluid, exhibiting properties of a viscous liquid as well as of an elastic solid. Such rheological properties are usually quantified by the two parameters viscosity and elasticity. While the former refers to the resistance of the fluid to flow, the latter describes the more solid like property of the material stiffness. Both parameters are complex quantities that depend on further parameters like temperature, shear rate, shear frequency, time and length scale etc. and can therefore only hardly be applied to grasp the complete behavior of such systems if evaluated without experimental details and boundary conditions. Nevertheless, viscosity and elasticity or derived parameters represent an established measure to describe rheological properties of mucus and are given by

$$\mu^* = \mu' - i\mu'' = \frac{\tau^*}{\gamma^* i\omega} = G' + iG'' \quad (1)$$

Here, μ^* is the complex viscosity with its real and imaginary part μ' and μ'' corresponding to the viscosity and the elasticity, τ^* = shear stress, γ^* = shear strain and G' and G'' represent storage and loss modulus respectively; μ is often denoted with the symbol η as

well. The viscosity of mucus ranges between 10^2 and 10^{-2} Pas (Lai, Wang et al., 2009), referring to ten to 100000 times that of water depending on the parameters mentioned above as well as disease state and species.

Not only within one species or even within one individual, the variation in the magnitude of the above mentioned parameters is significant, which demonstrates the highly heterogeneous nature of this fluid. This heterogeneity impedes general conclusions regarding the modeling and prediction of rheological behavior of mucus. It is however quite established that any disturbance in the homeostasis of mucus secretion (e.g. in CF) affects mucus rheology and thus mucociliary clearance of particles trapped inside the mucus blanket.

Before particles are cleared they make contact with the mucus blanket. Once submersed inside this hydrogel, particle mobility within this matrix and the mechanisms influencing the extent of this mobility are yet unsolved. Driving forces for a particle translocation into or even through this barrier are impaction, gravity, diffusion and external forces such as magnetic or electrostatic force fields. The first three of these mechanisms depend mainly on particle properties such as impaction trajectory and velocity, particle density, shape and size and rheological properties of the fluid. Diffusion behavior in dependency of particle properties is of great importance in the investigation of particle mobility in mucus. Diffusion in viscous fluids is a complex topic which demands sophisticated mathematical models. The most established model for diffusion is given by the Stokes-Einstein equation, relating particle size and diffusion constant

$$D = \frac{k_B T}{6\pi\mu r} \quad (2)$$

with D = diffusion constant, k_B = Boltzmann constant, T = temperature and r = particle radius. The diffusion constant describes how fast a particle diffuses. This can be seen by the relation between D and the mean squared displacement (MSD, $\langle \Delta r^2(t) \rangle$) for three-dimensional diffusion:

$$\langle \Delta r^2(t) \rangle_t = 6Dt^\alpha \quad (3)$$

Here, t represents the correlation time of the experiment while α has the value of 1 in a purely viscous fluid but can be different for complex fluids such as mucus or other hydrogels. In this case r denotes the distance from the location at the previous time step. The MSD is proportional to the width of the probability distribution of particle location (figure 5) i.e. it quantifies the probability to diffuse a certain distance within the given correlation time t .

However, as seen in equation 3, in particular for complex fluids, this determination of diffusion behavior is strongly dependent on the correlation time t , i.e. the time span for which the MSD is measured. Therefore, it is not easy to distinguish between different types of diffusion, such as hindered or free diffusion (figure 6) by only considering short correlation time spans.

Although being particularly important concerning the mobility of particles in mucus, this strict discrimination is therefore not often addressed in current research. Much more, the focus of studies investigating particle-mucus interactions has been laid on the mechanisms involved in the restriction of particle mobility. Here, the goal is in the determination of particle properties influencing the mobility such as adhesion to mucus or particle size. These parameters are important to describe the filtering ability of mucus as being primarily a size sieving (Sanders, Rudolph et al., 2009) or interaction filtering (Lieleg and Ribbeck, 2011) process. While the former model pronounces the sizes of the pores inside mucus or other biological hydrogels as limiting factor, the latter favors adhesive interactions between particles and gel components. Whatever mechanism will be dominant in the respective case, the reason will surely lay within the structure of mucus on the microscale which is -in detail- still not clear (Peppas and Huang, 2004). Unfortunately, recent studies relied only on microscopic analysis with rather harsh conditions or very indirect methods to clarify mucus structure. Therefore, the investigation of the structure of native pulmonary mucus in its physiological state is very important to understand particle mobility in mucus and their interactions with mucus components such as mucins.

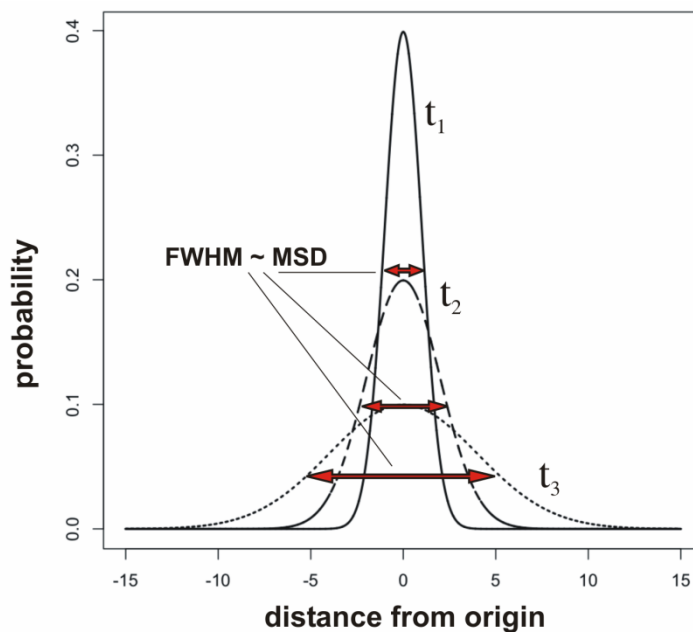


Figure 5: The meaning of the MSD can be visualized by plotting the probability of a particle to be located at a certain distance from the origin. With increasing time ($t_1 < t_2 < t_3$) this distribution broadens and the MSD, being proportional to the width (full width at half maximum, FWHM) of the distribution, increases. This means, the probability to find the particle away from the origin increases (as quantified by the MSD), whereas the origin is still the most probable location of the particle. Image by courtesy of Dominik Selzer.

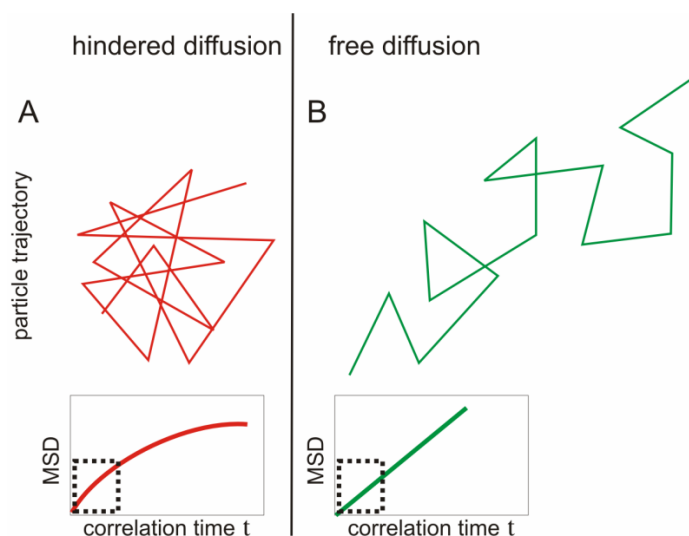


Figure 6: Free (B) and hindered diffusion (A) cannot easily be distinguished by MSD measurement. For short correlation times t (highlighted by the box) plateau values for the MSD are not reached, thus showing similar behavior for both types of diffusion behavior.

3.4 Aim of This Work

As presented in the previous sections, the thick mucus blanket and its clearance by ciliary action acts as significant barrier to the translocation of deposited particles down to the epithelium and thus the blood stream. The mobility of particles in mucus and the dependence of yet unknown parameters or the controllability of the mucociliary clearance are largely unexplored. Especially for pharmaceutical purposes intending to maximize such translocation, this is of great importance. However, it is not desired to decrease or even abort mucociliary clearance, as it is the primary innate defense mechanism in the lungs and thus crucial for pulmonary health. Due to the same reason, it is not desired to diminish the overall barrier properties of the pulmonary mucus. A much more elegant way to reach increased bioavailability of formulations administered via the lungs would be to circumvent mucociliary clearance on the individual particle level and to manufacture particles capable of a fast penetration through an unaltered mucus layer.

Not only for the reasons mentioned above but also for toxicological considerations it is absolutely crucial to first understand the interactions of particles with such non-cellular barriers of the lungs. Here, several still open questions remain and are tackled in the presented work:

- The study presented here aimed to give insight into the yet unknown dependence of the mucociliary clearance of particulate material on various particle properties such as size, shape, charge or surface properties to understand the mucociliary clearance on the microscopic level.
- Furthermore, the investigation of the process of particle sedimentation and impaction upon deposition onto the mucus blanket was expected to explain what happens between the events of particle deposition and mucociliary clearance of the particle.
- However, once deposited and while being transported via mucociliary clearance, it is still not clear if and by which mechanism (nano)particles may translocate through the mucus blanket, how this affects biodistribution of inhaled material and how this can be controlled by smart particle design. This is particularly important in terms of the connection between mucus' microstructure, diffusion and overall particle

retention in the lungs. Therefore, the mobility of particles once trapped inside the mucus blanket and their interactions with the mucus mesh were assessed. Here, not only (adhesive) interactions between particles and mucus components and diffusion, but also the response of nanoparticles suspended in mucus and model gels to external force fields and the implications on mucus structure on the microscopic level were investigated as they were hypothesized to play a crucial role for particle mobility.

4. Mucociliary Clearance of Nanoparticles

Parts of this chapter were published in:

Kirch, J., Guenther, M., et al. (2012). *Mucociliary clearance of micro- and nanoparticles is independent of size, shape and charge-an ex vivo and in silico approach.* J Control Release 159(1): 128-134

The first author contributed the following points to the publication:

- design, performance and interpretation of experiments
- writing of the manuscript

4.1 Abstract

The fate of inhaled particles after deposition onto the pulmonary mucosa is far from being solved, in particular with respect to mucociliary clearance and mucus penetration. Due to the fact that these phenomena govern pulmonary residence time and thus bioavailability, they are highly relevant for any kind of controlled release formulation delivered via that route. The work presented in the following section applied *ex vivo* approaches to investigate the dependency of muciliary clearance of micro-, submicron and nanoparticles on size, shape, charge and surface chemistry of such particles. In addition, measurement of mucociliary clearance of different particles also provided information about their penetration into mucus. Surprisingly, no significant differences in mucociliary clearance could be found for any type of particle under investigation. We hypothesized that particle penetration into the mucus gel layer is negligible at least within the time frame allowed by horizontal mucus transport. The presented data suggests that the observed lack of difference in mucociliary clearance is caused by the lack of immediate penetration of deposited aerosol particles into the mucus blanket.

4.2 Introduction

Before reaching the epithelial barrier, particulate drug carriers deposited onto mucosal tissues have to cross the mucus gel layer (Khanvilkar, Donovan et al., 2001; Cone, 2009; Sanders, Rudolph et al., 2009). In the context of local pulmonary drug delivery in the upper lungs, rapid mucociliary clearance of trapped drug carriers will put a serious limitation to any attempt of designing inhalable controlled release systems. Strategies to control the mucociliary clearance of pulmonary drug carriers without jeopardizing the important barrier function of pulmonary mucus e.g. by innovative particle design, therefore need to be addressed first, both scientifically and technologically.

Mucociliary clearance dramatically influences the fate of deposited drug carriers: Inhaled particulate material is trapped and moved along with the moving mucus to be excreted by transport to the larynx (Iravani and Melville, 1976; Fulford and Blake, 1986; Antunes and

Cohen, 2007). Those processes have long been under investigation (Geiser, Cruz-Orive et al., 1990; Geiser, Serra et al., 1995; Geiser, Im Hof et al., 1997; Geiser, Gerber et al., 2000), but are still not fully understood. In previous studies, the focus has mainly been laid on the macroscopic investigation of processes and parameters which influence the regulation of mucus secretion (Boucher, 2007) and clearance (King, 2006). Here, characterization of mucociliary clearance in healthy and diseased state (Donaldson, Corcoran et al., 2007; Livraghi and Randell, 2007) and under pharmacologically relevant conditions (Bennett, 2002) plays a large role in current research.

Translocation of particles through pulmonary mucus has not been satisfactorily clarified so far, especially considering the fact that the pulmonary mucus blanket is continuously moving due to mucociliary clearance. This is particularly true for nanosized particles which are much smaller in diameter than the thickness of the mucus blanket.

Considering the interaction of particles with a moving gel layer, it is not clarified yet, how such a translocation can be correlated with dynamic processes of the ciliary propulsion of this moving layer (e.g. fluid dynamics) as well as particle properties such as size, shape, charge and surface chemistry. Therefore, the aim of this study was to investigate and possibly identify critical particle properties which may influence their mucociliary clearance and translocation within the mucus blanket. Measuring the mucociliary clearance velocity of particles may also give insight into their penetration behavior into mucus: Whereas non-penetrating particles will be cleared with the moving mucus (figure 7A), particles that cross the mucus layer or even make contact with the epithelium (figure 7B) will on average be slowed down as they reach layers of smaller flow velocity (PCL and vicinity of the epithelium). Thus, they will show no, or at least a decreased average clearance velocity, which can be measured by particle tracking.

The influence of particle properties, such as surface chemistry, size, charge and shape on mucociliary clearance (and indirectly on penetration potential) can be determined experimentally by the recently described *ex vivo* Embryonic Chicken Trachea (ECT) model (Henning, Schneider et al., 2008; Henning, Schneider et al., 2010) where horizontal particle trajectories can be imaged and analyzed. To improve comparison of clearance velocities of different particles and to reduce the statistical individual variance, we successfully applied a method to track particles of different type simultaneously.

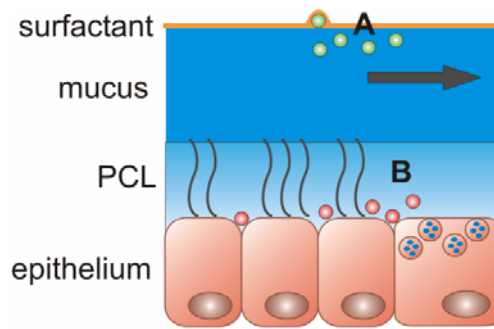


Figure 7: Non-penetrating particles (A) will be cleared with the moving mucus blanket. Penetrating particles (B) will, on average, be transported slower or even not at all by translocating to areas with negligible horizontal mucus velocity such as the vicinity of the epithelium.

4.3 Experimental

4.3.1 Materials

Experiments were conducted with three main groups of particles: Size dependency was investigated with differently sized polystyrene (PS) particles, shape and charge dependency was analyzed with differently charged (COOH surface or polyethylenimin (PEI) coating, respectively) rod-shaped (aspect ratio ≈ 4) and spherical PS particles. Dependency on surface chemistry was investigated with maghemite particles of different surface chemistry.

Spherical PS-COOH particles (nominal density $\rho_p = 1050 \text{ kg/m}^3$) were purchased from BangsLabs (Fishers, USA), rod-shaped particles were made by stretching spherical PS-COOH particles purchased from Polysciences (Warrington, USA) according to the film stretching procedure previously described (Champion, Katare et al., 2007). PEI was coated on particle surface through passive adsorption: Particle suspension (10^8 particles/ml) was incubated 1:1 in 2 mg/ml PEI solution overnight with end-to-end mixing. Particles were washed two times in phosphate buffered saline (PBS, 5 mM) and stored at 4 °C. Washing was performed by 15 min centrifugation at 7000 rpm and subsequent resuspension. Maghemite particles were obtained from Chemicell (Berlin, Germany), had a mean density of $\rho_p = 1250 \text{ kg/m}^3$ and were assembled from 20 nm subunits. All particles, except for rod-

shaped and PEI coated particles were purchased from commercial sources. Fluorescent label was fluorescein isothiocyanate (FITC) or 4',6-diamidino-2-phenylindole (DAPI) for reference particles, respectively, incorporated in the polymer matrix of the PS particles by the manufacturer.

Maghemite particles, were coated with a lipophilic dye by the manufacturer. Subsequently, a second layer enveloping the particle with a hydrophilic polymer was attached by the manufacturer to protect the particles against aggregation by foreign ions (Tseng, Di Carlo et al., 2009; Cinti, Taranta et al., 2011). All chemical modifications were linked covalently to the surface of maghemite particles by the manufacturer (chitosan, starch, phosphatidylcholine (PC), polyacrylamide (PAA)). PS-COOH particles of 555 nm hydrodynamic diameter were applied as reference particles in all experiments. All chemicals used were of analytical grade and purchased from standard commercial sources. Fertilized eggs, specified as pathogen free, were obtained from Lohmann (Cuxhafen, Germany).

4.3.2 Particle Tracking Experiments

In the ECT model, particles were deposited onto excised trachea from chicken embryos. Particle movement was monitored by optical means. In this study, fertilized eggs were incubated for 18-19 days at 37 °C and 60 % humidity in a breeding chamber. Trachea were excised and particles deposited as described earlier (Henning, Schneider et al., 2008). Briefly, after isolation, trachea were cut into half pipes and aqueous particle suspension was deposited on their inner (mucosal) side by using a MicrosprayerTM (PennCentury Inc., Wyndmoor, USA) as displayed in figure 8. Particles were applied as a mixture of two different types of particles suspended in millipore water; in each case PS-COOH particles of 555 nm hydrodynamic diameter were used as a reference particle. The applied amount of particle suspension was approximately 0.1 µl (0.04-0.06 % solid fraction) per trachea.

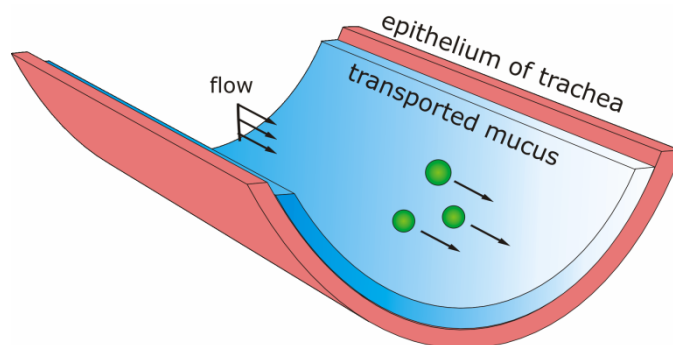


Figure 8: Trachea were cut in half pipes and particles are deposited on top. Trapped particles (green) are transported horizontally by mucociliary clearance and can be tracked by fluorescent labeling.

With an assumed joint thickness of 20 μm for PCL and mucus layer, the amount of liquid on top of the tracheal epithelium is 1.6 μl (taking into account average length and diameter of embryonic chicken trachea). The application of the particle suspension therefore represents the addition of 6.25 % fluid. According to previous studies (Powell, Aharonson et al., 1974) this was assumed not to influence the rheological properties of mucus significantly. Throughout the experiment, the half pipes were placed onto Locke-Ringer solution soaked tissue. After particle deposition, the half pipes were transferred into a humidity (99 %) and temperature (33 $^{\circ}\text{C}$) controllable chamber. Particle transport velocity due to mucociliary clearance was measured by fluorescence microscopy (Axioimager, Zeiss, Jena, Germany). Clearance rates measured by this method are comparable to human clearance rates (Henning, Schneider et al., 2008) which range between 3-25 mm/min (Hofmann and Asgharian, 2003; Antunes and Cohen, 2007) All particles were fluorescent-labeled to allow tracking of their transport in the x - y plane. Reference particles and particles under investigation were labeled with a different fluorophore and could therefore be distinguished. Particle trajectories were recorded as image sequences of 10 s length. Due to the fact that most particles left the frame after this time, longer sequences could not be imaged. Several sequences were recorded on different spots on each trachea and particle trajectories were analyzed. On average, 10-20 particle trajectories per sequence were analyzed. To investigate the dependency of transport velocity on particle shape, spherical and rod shaped PS particles were applied and tracked simultaneously. To investigate charge dependency of transport velocity, reference particles were applied and tracked

simultaneously with positively or negatively charged rod shaped and spherical particles, respectively. To complete these studies, the dependency of transport velocity on particle surface chemistry was investigated with maghemite particles coated with chitosan, PC, PAA and starch. In each case, the particle type under investigation was applied and tracked simultaneously with reference particles or compared directly (e.g. in the case of shape dependency). The mean transport velocity of each type of particle was calculated by MtrackJ software. The mean transport velocity of the reference particles in each sequence was set to 100 %. For each sequence, the mean transport velocity of reference particles was compared to the mean velocity of the particle type under investigation.

4.3.3 Particle Characterization

Particles were characterized by dynamic light scattering (DLS), scanning electron microscopy (SEM) and atomic force microscopy (AFM). DLS measurements were conducted with particle suspensions in millipore water with a Zetasizer Nano-ZS (Malvern Instruments, Herrenberg, Germany): Here, particle solutions provided by the manufacturer were diluted with millipore water to yield concentrations of approximately 10^8 particles per ml. SEM measurements were conducted with a JSM 7001F Field Emission SEM (Jeol, Tokyo, Japan) under high vacuum conditions and room temperature. Prior to scanning by SEM, particles were sputter-coated with gold (layer thickness approximately 10 nm). Accelerating voltage was 20 kV with a focal distance of 10 mm. Samples for microscopic imaging were prepared by coating freshly cleaved mica with aqueous particle suspensions (1:100 dilution of stock solution provided by the manufacturer) followed by gentle drying with compressed air. AFM scans were done using a Multimode V (Veeco, Plainview, USA). Particles were scanned using non-contact mode and scan rates of 0.7 Hz. Standard non-contact mode cantilevers were used to image dried particles on mica (OMCL-AC160TS, Olympus, Essex, Great Britain).

4.4 Results

4.4.1 Particle Characterization

Characterization of the particles by DLS showed that all particles were monodisperse (table 1) with the criterion for sufficient monodispersity being a polydispersity index (PDI) below 0.2. Measurement of zeta potential could confirm the charge given by the manufactures as either clearly positive, negative or neutral. Visualization by microscopic means was used to examine morphology of the particles and to estimate values of size and dispersity as measured by DLS. Rod shaped particles could not be measured by DLS because this technique incorporates spherical particles as boundary condition and thus gives misleading results for nonspherical particles. Figure 9 displays AFM and SEM images of PS spheres, PS rods and maghemite particles. SEM and AFM data were in accordance with values measured by DLS. Maghemite particles show greater polydispersity as proposed by DLS data. Disintegration of maghemite particles (which had been assembled from smaller subunits) due to dehydration effects during sample preparation can apparently not be avoided completely. The assembly of the maghemite particles from smaller subunits (“multi domain magnetic core” as specified by the manufacturer) can be seen by the cluster-like appearance of the particles. PS particles seem much smoother and display very low polydispersity.

Table 1: Particle characterization by DLS. All particle types show sufficient monodispersity (* indicates measurement in millipore water).

	Particle chemistry	Size [nm]	Zeta potential * [mV]	PDI [a.u.]
maghemite particles	chitosan	146.0 ± 0.5	40.1 ± 0.9	0.1 ± 0.01
	PC	160.6 ± 0.6	-39.9 ± 1.9	0.07 ± 0.01
	starch	176.5 ± 1.2	-0.9 ± 0.1	0.09 ± 0.02
	PAA	197 ± 1.5	-32.7 ± 0.8	0.12 ± 0.02
	uncoated maghemite	165 ± 0.7	38 ± 1.1	0.14 ± 0.03

PS	555 ± 6.3	-49.5 ± 0.4	0.04 ± 0.07
(reference particle)			
PS (“200 nm”)	248.3 ± 1.4	-44.9 ± 0.4	0.004 ± 0.002
PS (“1000 nm”)	926 ± 115	-32.4 ± 0.8	0.17 ± 0.09
PS (“6000 nm”)	6242 ± 469	-32.7 ± 0.7	0.09 ± 0.07
PEI-terminated PS (positively charged spheres)	600.5 ± 7.0	41 ± 2.0	0.14 ± 0.08
COOH-terminated PS (negatively charged spheres)	555 ± 7.0	-42 ± 2.1	0.06 ± 0.03

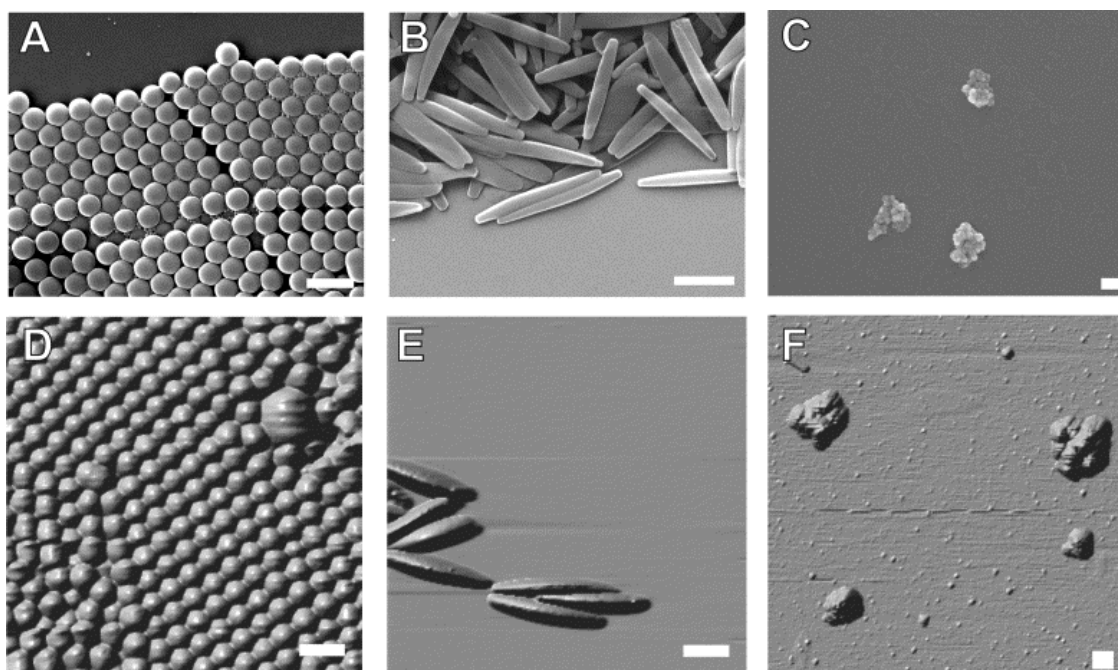


Figure 9: SEM (A-C) images as well as AFM images (D-F) of spherical and rod shaped PS particles (A, B, D, E) and maghemite particles (C, F). Maghemite particles show rougher surface and more heterogeneous shape than PS particles. Scale bar represents 1 μm for PS particles or 100 nm for maghemite particles.

4.4.2 Particle Tracking Experiments

The ECT model was employed to visualize and analyze the transport of deposited particles by mucociliary clearance. Particle trajectories showed the effective and well directed clearance of trapped particles (figure 10). Particles were transported mainly homogeneously throughout the imaged sequences. Slight divergences in direction or velocity of transport by mucociliary clearance were probably caused by the convergence of different metachronal fields. Trachea with impaired ciliary activity could be distinguished by strongly heterogeneous, circular or even reverse particle transport.

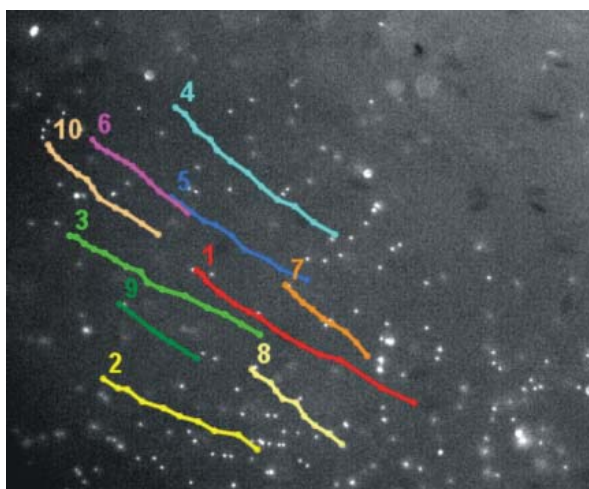


Figure 10: Trajectories of particles transported by mucociliary clearance. Slight differences in transport direction may be caused by the convergence of metachronal fields. Single trajectories (numbered) are shown in different color. Image size is 120 μm in width.

The aim of this study was to investigate the influence of different parameters such as shape, size, charge and surface properties on the clearance behavior of micro- and nanoparticles after deposition. In this context, clearance transport velocity of different types of particles was analyzed. No significant difference in transport velocity between reference particles and particle type under investigation could be found for any data set, be it dependency on size, charge, shape or surface chemistry (One Way ANOVA-Sigma Plot, systat, Chicago, USA). To exclude a retarding influence of PS reference particles on mucus

clearance, chitosan coated and starch coated maghemite particles were compared by applying a different type of reference particle (maghemite uncoated). Again, the compared types of particles did not show a significant difference in mean transport velocity. Results regarding the possible dependency of clearance transport velocities of particles under investigation on particle size, charge, shape and surface chemistry are summarized in table 2. Comparably high error in table 2F is probably due to smaller sample size ($n_{\text{trachea}} = 3$). Although most particle ensembles were transported as uniform formation, demonstrating complete immobilization in the mucus blanket with little relative trajectories to each other, few particles in deeper layers could be observed. The magnitude of this effect was independent of particle characteristics and may indicate the existence of voids inside the mucus blanket.

Table 2: Relative mucociliary clearance velocities of particles under investigation. Transport by mucociliary clearance is independent of particle size (A), shape (B), charge (rod shaped particles (C), spherical particles (D)) and surface chemistry (E). A retardation of all particles by PS reference particles may be excluded: The application of a different type of reference particle reproduces previously found velocity relations (F). Values are means \pm CV, (trachea: $n \geq 4$ (A-E), $n = 3$ (F); particles: $n \geq 100$).

Size dependency of clearance velocity (A)		
Particle	Relative difference of transport velocity to reference particle [%]	Statistical error [CV]
200 nm	2.7	10.7
1000 nm	2.1	8.9
6000 nm	-6.0	8.8
Shape dependency of clearance velocity (B)		
Particle	Relative difference of transport velocity to reference particle [%]	Statistical error [CV]
Rods	4.2	17.9
Spheres	0 (reference)	
Charge dependency of clearance velocity (rod shaped particles) (C)		
Particle	Relative difference of transport velocity to reference particle [%]	Statistical error [CV]
rods (+)	2.8	6.4
rods (-)	7.6	11.5

Charge dependency of clearance velocity (spherical particles) (D)		
Particle	Relative difference of transport velocity to reference particle [%]	Statistical error [CV]
spheres (+)	2.2	9.1
spheres (-)	0.5	8.1
Dependency of clearance velocity on surface chemistry (E)		
Particle	Relative difference of transport velocity to reference particle [%]	Statistical error [CV]
PC	-1.0	6.8
chitosan	0.5	8.1
starch	1.7	6.0
PAA	10	14.0
Dependency of clearance velocity on surface chemistry (influence of reference) (F)		
Particle	Relative difference of transport velocity to reference particle [%]	Statistical error [CV]
chitosan	11.6	42.6
starch	8.2	23.9

4.5 Discussion

The presented study describes the investigation of trajectories of individual particles upon impaction onto the mucus layer. This process is rather fast and horizontal transport by mucociliary clearance governs the order of magnitude of the relevant velocities. ECT experiments showed that relative clearance velocity of the particles under investigation did not differ from that of simultaneously measured reference particles. This simultaneous measurement allowed for a direct comparison of reference particles and particles under investigation. A dependency of shape, size, charge or particle coating on the relative transport velocity was not observed. Therefore, the clearance behavior and the transport velocity of particles deposited onto the mucus blanket seems to be mainly determined by the characteristics of the underlying mucus and its flow properties.

Experimental and theoretical studies (Matsui, Randell et al., 1998; Smith, Gaffney et al., 2007; Smith, Gaffney et al., 2008) predicted heterogeneous flow velocities along the height of the mucus layer with smaller average velocities in the region of the PCL, the vicinity of the epithelium and finally vanishing flow at the epithelium. Therefore, penetrating particles will on average experience a decreased flow velocity and thus slower transport while advancing deeper towards the epithelium (figure 7). This is the reason for mucociliary clearance velocity of deposited particles being able to provide information about the penetration potential of such particles. Taking into account the presented results, the mentioned particle properties might thus not influence particle penetration.

However, we have so far not considered the role of wetting and diffusion: It is well known from previous studies that wetting is a strong driving force to submerge particles in biological fluids (Gehr, Green et al., 1996; Gehr, Im Hof et al., 2000; Fiegel, Jin et al., 2005). Although this behavior might not be influenced by shape, surface topography or surface free energy (Geiser and Kreyling, 2010) its influence on particle penetration can be important. It could previously be demonstrated that the existence of a surfactant lining strongly influences the immersion of particles into airway fluids (Schurch, Gehr et al., 1990; Gehr, Green et al., 1996; Fiegel, Jin et al., 2005). The force caused by the interplay of particle wetting and surface tension of the surfactant layer can be strong enough to result in the displacement of the particle into the epithelium. From the physical point of view, it is important to stress that this particular effect only comes to pass (and has so far only been reported (Geiser and Kreyling, 2010)) if the particle size approaches the thickness of the fluid layer. In the scenario described here, smaller particles (especially submicron or nanosized particles) are deposited onto airway fluids. For those small particles, the described forces can maximally immerse the particle completely but cannot contribute to any further displacement within the mucus layer.

Overall the presented results lead to the conclusion that the particle properties under investigation (size, shape, charge, surface chemistry) play only a minor role in their clearance behavior, i.e particles that are trapped in the mucus will be cleared at a velocity that is equal to the clearance velocity of the mucus, independent of particle properties. However, the mucus blanket does not appear totally uniform, either in surface coverage as well as in thickness (van As and Webster, 1972; Iravani and Melville, 1976; Sims and Horne, 1997). Therefore, besides fast penetration through the mucus blanket, the deposition on poorly covered patches of the epithelium (van As and Webster, 1972;

Moller, Felten et al., 2008; Geiser and Kreyling, 2010) followed by epithelial adhesion represents a further possibility to escape the mucociliary clearance. The latter phenomenon, although there has been extensive proof for such heterogeneity of the mucus blanket in thickness and coverage of the epithelium (Iravani and Melville, 1976; Im Hof, Gehr et al., 1997; Sims and Horne, 1997), is not easily accessed and has so far rarely been exploited for pharmaceutical purposes. Nanoparticles deposited on such patches of the epithelium which are only poorly covered with mucus, can slip through these voids inside the mucus blanket and reach the PCL or even the epithelium. The existence of a fraction of particles which may undergo this process was observed in this study and this may also be the reason for the discrepancy between fast horizontal transport of individual particles and previously reported long term (> 24 h) retention of fractions of inhaled nanomaterial (Moller, Felten et al., 2008) (with a clearance velocity of 2 mm/min particles deposited in the airways should be cleared from the lungs within maximally 2 h). Hence, for pharmaceutical applications, the more passive approach of enhancing the adhesion of particles to the epithelial cell surface as shown by Fischer et al. (Fischer, Aleman et al., 2009) deserves high attention. The experimental results described here clearly suggest that in quantitative terms of particle retention in the airways, this mechanism of translocation may be at least equally important than direct particle penetration through mucus; an approach which combines these mechanisms is considered ideal.

In further studies, the role of mucus fluid dynamics and microstructure in the directed, vertical translocation of particles should be investigated: Here, not the local particle mobility and diffusion (Sanders, De Smedt et al., 2003; Lai, O'Hanlon et al., 2007; Lai, Wang et al., 2009; Sanders, Rudolph et al., 2009) as usually described by quantifying the mean-squared displacement of particles (Valentine, Perlman et al., 2004; Lai, O'Hanlon et al., 2007; Crater and Carrier, 2010) should be measured; rather should it be cleared if voids inside the mucus blanket in its *in vivo* state are possibly interconnected and if and under which preconditions they allow particle translocation. Furthermore it should be clarified, how particle impaction and their trajectories influence sedimentation of deposited particles in mucus. Here, the underlying physical principles have been seldom considered in previous studies but need to be characterized first, before being able to describe particle-mucus interactions satisfactorily. These points are further assessed in the following sections.

4.6 Conclusion

In summary, clearance velocity of micro-, and nanoparticles, trapped in the pulmonary mucus blanket and transported by mucociliary clearance, was shown to be independent of size, shape, charge and surface properties of the particles under investigation. Direct comparison of transport velocities of simultaneously measured particle types allowed for an estimation of particle penetration through the mucus blanket, revealing that vertical penetration of particles into the mucus blanket may be negligible compared to their horizontal transport due to mucociliary clearance. Possible strategies to design particles capable to escape the otherwise very effective mucociliary clearance remain either a substantial increase in their diffusivity in mucus (mucopenetration), or minimizing mucoadhesion, targeting possible voids in the mucus blanket and seeking direct bioadhesion to the epithelial surface. Such a substantial increase in diffusivity or mobility of particles in mucus may be reached by the application of external forces to pull the particles through mucus. Before such approaches can be realized, however, the process of sedimentation in and impaction onto the mucus blanket of nanoparticles have to be clarified. Furthermore, mobility of particles inside the mucus mesh and the implications of mucus' microstructure on such mobility have to be investigated.

5. Fluid Dynamics of Particle-Mucus Interactions

Parts of this chapter were published in:

Kirch, J., Guenther, M., et al. (2012). *Computational fluid dynamics of nanoparticle disposition in the airways: mucus interactions and mucociliary clearance*. Comput Visual Sci: accepted

The first author contributed the following points to the publication:

- design and interpretation of simulations and analytical solutions
- writing of the manuscript

The second author of the publication performed simulations and calculations.

5.1 Abstract

Interactions of nanoparticles with respiratory fluids such as pulmonary mucus are currently under investigation and are involved in a variety of applications. The clearance processes especially for nanoparticles are still not fully understood. The study presented in the following section represents an approach to describe deposition, sedimentation and clearance of nanoparticles within mucus with numerical and analytical models. Here, the physical background of nanoparticle behavior in fluid flow was taken into account for the first time within this context. Particle impaction as well as sedimentation and mucociliary clearance were simulated with computational fluid dynamics (CFD) and described analytically. Furthermore mucus plasticity as pathway for complex particle translocation was simulated using advanced CFD methods. We could demonstrate that fluid dynamics strongly influence the fate of deposited nanoparticles in mucus: Sedimentation and impaction were shown to be unlikely to contribute to particle translocation. However, intrinsic plasticity of mucus slabs and collision of such slabs may enhance particle translocation towards the pulmonary epithelium.

5.2 Introduction

This study aims to describe interactions of nanoparticles with mucus as the major non-cellular element of the mucosal barrier. Mucus is a complex fluid containing hydrogel-forming glycoproteins (mucins) and forms a compact barrier in the upper lungs. It has a very active role in the protection from inhaled material: Material deposited in the lungs usually adheres to mucus and can therefore be transported cranially and finally be excreted. This process is called mucociliary clearance.

Elimination of particulate matter by this mucociliary escalator reduces residence time and thus the amount of the drug at the site of action. Therefore, current approaches to increase bioavailability aim to enhance penetration of mucus by particles. On the other hand, one aims to increase the probability that particles remain at the deposition site (which seems only feasible if deposited on patches not covered with mucus). Which approach may be

favorable is not clear yet. Recent publications have described nanoparticle mobility in mucus depending on particle surface chemistry (Lai, Wang et al., 2009). However, those approaches solely rely on investigations concerning the MSD of particles already submersed in mucus but do not take into account any clearance processes or deposition effects. Although these processes have been under experimental investigation for quite long time (Geiser, Cruz-Orive et al., 1990; Geiser, Im Hof et al., 1997; Geiser, Gerber et al., 2000) they are still largely unexplored. The aim of this study was the description of particle deposition onto mucus with computational methods to clear if particles deposited onto the mucus blanket are able to cross the mucus layer and reach the underlying epithelium by impaction or sedimentation. In addition, the applicability of an analytical solution to the problem was investigated. The aim of such numerical and analytical approaches is the development of a model which allows for a quick estimation of particle-mucus interactions in terms of particle trajectory inside the mucus blanket upon the deposition. This is necessary because it is seldom known how all physical interactions that are involved in particle displacement balance and thus determine the behavior of deposited particles of different properties. Furthermore, mucus plasticity was analyzed by CFD to assess additional possibilities of particle attachment or translocation to the epithelium (figure 11): It is known that the mucus blanket is heterogeneous not only in thickness but also in surface coverage, transport velocity and direction (Iravani and Melville, 1976). Therefore, mucus droplets of potentially even varying size may collide if being transported within different metachronal fields. Upon such collisions, particles deposited on the mucus blanket may be submerged and pushed deeper inside the mucus layer and may thus encounter the epithelium in the end. Another possibility of particles reaching the epithelium besides diffusion and impaction is the translocation due to mucus spreading: Mucus droplets, either directly upon secretion or after separation from larger entities, may spread if no confining barriers are located on the sides. This spreading was modeled to determine the magnitude of the time spans of such spreading phenomena and to find out if this behavior can indeed contribute to particle translocation to the epithelium.

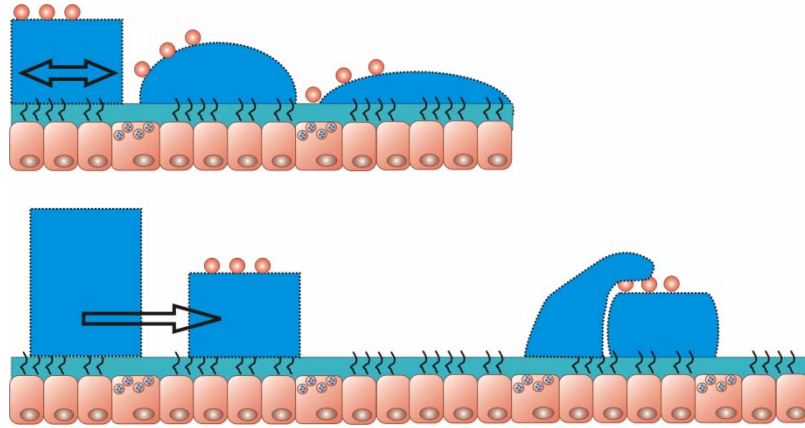


Figure 11: Mucus plasticity due to spreading (top) and deformation upon collision of mucus slabs (bottom) may be the reason for particle translocation to the epithelium: Particles deposited on top of the mucus blanket will get into close contact of the epithelium during the spread of the mucus droplet. Collision may cause immersion of particle into the depth of the mucus layer.

5.3 Experimental

5.3.1 CFD and Analytical Solution of Particle Trajectories

5.3.1.1 Computational Model

To simulate particle deposition on top and sedimentation within the mucus layer a 2D model was applied. The plane chosen was orthogonal to the mucus and parallel to the mucus flow. The computation domain (figure 12) used was quadratic and had a side length of $100\ \mu\text{m}$. Numerical computation of the fluid flow and the particle dynamics was done by the commercial CFD tool Ansys Fluent 12.1 with an underlying regular rectangular numerical grid. For the upper and lower boundary, a no-flux boundary was set. On the upper boundary that represents non-moving air, the velocity is set to be zero. The lower boundary simulates propulsion of mucus by cilia by a moving wall approach. Here, a constant velocity was assumed as first approximation. All other boundaries were periodic. The hereby simulated flow was a multiphase flow, where air, mucus and particles are different phases. The interface between the air and the mucus phase is a so-called free

boundary, i.e. no shape can be prescribed. The shape of the interface is the result of several balanced forces. We could expect that the interface is a straight line since there is no force which might destroy this line shape. Hence, the surface tension could be neglected in this section. The simulations were done using the volume-of-fluid (VOF) model (Hirt and Nichols, 1981) to take into account the free boundary. The simulation of the particles' paths was done by a Lagrangian method using Fluent's discrete phase model (DPM). For the numerical as well as the analytical model viscosity of the mucus layer increased according to physiological values from 1 mPas at the bottom to 6 Pas (Lai, Wang et al., 2009) at the mucus/air interface to represent gradual transition of the watery PCL to highly viscous mucus layer (Randell and Boucher, 2006). Determination of mucus flow velocity $u(z)$ was achieved by simulating mucus flow as steady-state process. Particle motion inside mucus after impaction onto this fluid layer, however, is a non-steady-state process with adapted time step control. Maximum resolution in time was 2.2×10^{-9} s. Convergence was surveyed by monitoring the decrease of residuals. Here, a decrease of residuals to a plateau value of 10^{-6} was accepted as convergence criterion for all simulation results.

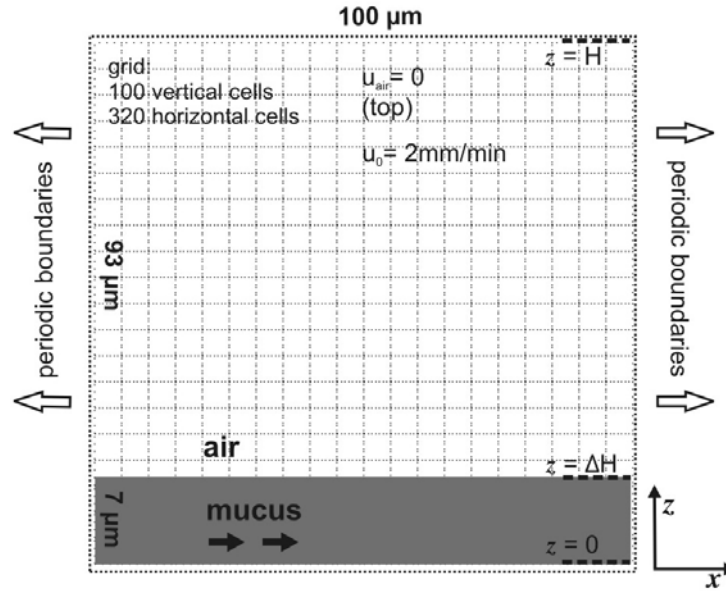


Figure 12: Computation domain of particle mucus interactions displaying both phases (mucus and air). Boundaries are periodic and the grid consisted of 100 vertical and 320 horizontal cells.

5.3.1.2 Analytical Model

In order to find the basic equation describing mucus flow only the important forces and effects had to be considered. By neglecting all terms not relevant for the described situation, the Navier-Stokes equation could be solved analytically. Due to the fact that propulsion of the mucus layer is uniform and continuous, the flow can be considered to be stationary. Additionally, as velocity and pressure are low the fluid can be considered to be an incompressible fluid. Further simplification could be made considering the Reynolds number. With the height of the mucus layer as the characteristic length a very small Reynolds number was obtained, as the height is small and the viscosity is rather high i.e. inertial forces are very small compared to the viscous forces. Therefore a laminar flow without turbulence could be assumed and the flow could be described by the stationary Navier-Stokes equation:

$$-\nabla p + \nabla[\mu(\nabla \vec{v} + (\nabla \vec{v})^T)] + \vec{f} = 0 \quad (4)$$

Here, p represents the pressure, $\mathbf{v} = (u, k, w)^T$ the velocity, μ the viscosity and \mathbf{f} additional volume forces. In non-newtonian fluids the viscosity is usually dependent on $\partial u / \partial z$. Here we could approximate by using $\mu = \mu(z)$ which yields the same results if $\partial u / \partial z$ is linear. In the following, direction parallel to the mucus is denoted with x and the direction orthogonal to the mucus with z . The y -direction was not considered as the computation domain was chosen parallel to the flow direction. First, it could be assumed that the boundary conditions and the fluid properties in the x -direction are uniform and do not change in time. Furthermore, the pressure gradient in this direction is zero. That means all quantities do not depend on the position on x -direction. All these assumptions allowed for writing the equation for the velocity in x -direction u in the following form:

$$\frac{\delta}{\delta z} \left(\mu(z) \frac{\delta u(z)}{\delta z} \right) = 0 \quad (5)$$

Further simplification was included with respect to diffusion or Brownian motion of particulate matter: For spherical particles, the time $t(\mathbf{b}, \mathbf{b}_0)$ required to reach the cilia by Brownian motion is

$$\tau(b, b_0) = \frac{2bb_0 - b_0^2}{2D} \quad (6)$$

with b = thickness of mucus, b_0 = starting height of the particle trajectory. D is given by equation (2). Mucus viscosities range between 10^2 and 10^{-2} Pas (Lai, Wang et al., 2009). Therefore we could determine a diffusion coefficient for a viscosity of 50 Pas which lead (with an assumed thickness of 10 μm for the mucus blanket) to a value of $t(10 \mu\text{m}) = 1.1 \times 10^6 \text{ s}$ (= 12.9 days). Even for highly diffusive particles (Lai, O'Hanlon et al., 2007) with $t(10 \text{ mm}) = 500 \text{ s}$, mucociliary transport velocity (typical value in *ex vivo* experiments: 2 mm/min) exceeds diffusional transport by far. Therefore it is plausible to neglect diffusional transport through the mucus blanket in a simple analytical model. Applied variables and parameters are summarized in table 3.

Table 3: Applied variables and their denotations

Variable	Denotation
p	pressure
μ	viscosity
v	flow velocity
u, k, w	flow velocity in x, y, z direction
V	particle velocity
U, K, W	particle velocity in x, y, z direction
u_M, u_A	flow velocity in mucus or air respectively
u_0	drive velocity of the mucus layer
r	particle radius

5.3.2 Simulation of Mucus Plasticity

Numerical simulations of mucus plasticity and mucus slab deformation were done using the software tool Finite-Pointset Method (FPM) recently developed at the Fraunhofer-Institute for Industrial Mathematics in Kaiserslautern, Germany (Tiwari and Kuhnert, 2002; Tiwari, Hietel et al., 2006). FPM solves fluid dynamic problems and its numerics are based on a grid-free method, i.e. unlike other CFD tools like Fluent, FPM needs no mesh to

discretize fluid mechanics equations but utilizes virtual particles which are transported with the fluid flow and act similar to fluid elements (Tiwari and Kuhnert, 2002). One major advantage of the method is the treatment of free boundaries as surfaces of the described mucus. A 2D-model of a mucus slab with a width of 20 μm and a height of 10 μm was considered here. The friction force between the mucus and its underground cannot be determined exactly, however the composition and nature of the underlying watery PCL is known. Although the fluid within the PCL is not very viscous, support by constantly beating cilia, secretion and absorption mechanisms and macromolecular structures enables it to be retained as distinct layer. Therefore, we placed the mucus slab on a 60 μm wide and 5 μm high layer of the same material but higher viscosity. This was done to result in a non-moving stable substrate with, however, similar interfacial properties to simulate underlying PCL. Mucus density was chosen to be 1000 kg/m^3 with a viscosity of 6 Pas (Lai, Wang et al., 2009). The viscosity of the underlying substrate was chosen 10 times larger. The temperature influence was not regarded. The resolution can be expressed by mean distance of virtual particles which is 0.13 μm in this case. As a solver for non-stationary problems, convergence is surveyed in each time step. The intrinsic convergence level for the equation solver is implied by the developer and the magnitude of this parameter cannot be given here.

5.4 Results

5.4.1 Particle Trajectories

5.4.1.1 Analytical Solution

In order to find an analytical solution the domain was divided into the mucus domain (M) and the air domain (A). Mucus is located in the height $0 < z < \Delta H$, the air domain is located in the height $\Delta H < z < H$, where H is chosen large compared to ΔH . The velocities are denoted by $\mathbf{u}_M(z)$ and $\mathbf{u}_A(z)$ for the flow velocity in mucus and in air, respectively. The general solution of the Stokes equation could be obtained by integrating the equation two times:

$$\mu(z) \frac{\delta u(z)}{\delta z} = C_1 \quad (7a)$$

$$u(z) = C_1 \int_{z_0}^z \frac{1}{\mu(z')} dz' + C_2 \quad (7b)$$

For the velocities in mucus and air following equations could be obtained:

$$u_M(z) = C_1 \int_{z_0}^z \frac{1}{\mu_M(z')} dz' + C_2 \quad u_A(z) = C_3 \int_{z_0}^z \frac{1}{\mu_A(z')} dz' + C_3 \quad (8)$$

It can be assumed that the viscosity of air is almost constant so that the equations could be simplified to

$$u_M(z) = C_1 \int_{z_0}^z \frac{1}{\mu_M(z')} dz' + C_2 \quad u_A(z) = C_3 z + C_4 \quad (9)$$

It remained to determine the unknown constants **C1**, **C2**, **C3**, **C4**. The complete solution could be obtained by choosing boundary and interface conditions. Therefore, the drive velocity of cilia was chosen as u_0 . Finally, the following velocities could be obtained:

$$u_M(z) = u_0 \frac{\mu_A \int_0^z \frac{1}{\mu} dz'}{H + \Delta H - \mu_A \int_0^{\Delta H} \frac{1}{\mu_M(z')} dz'} + u_0 \quad (10a)$$

$$u_A(z) = \frac{u_0}{H + \Delta H - \mu_A \int_0^{\Delta H} \frac{1}{\mu_M(z')} dz'} (z - H) \quad (10b)$$

These two equations describe flow velocity $u(z)$ of the mucus layer and the air above. The analytical solution of the flow velocity of the mucus layer $u_M(z)$ is compared to its numerical solution in figure 13. These results qualitatively match experimental (Matsui, Randell et al., 1998) as well as numerical results of previous studies which apply much more complex models for the ciliary drive of the mucus layer (Smith, Gaffney et al., 2007; Smith, Gaffney et al., 2008). Similar to those studies, mucus flow velocity was found to be almost constant along the mucus' height. The knowledge about flow velocities of mucus depending on z was used to describe particle trajectories after deposition.

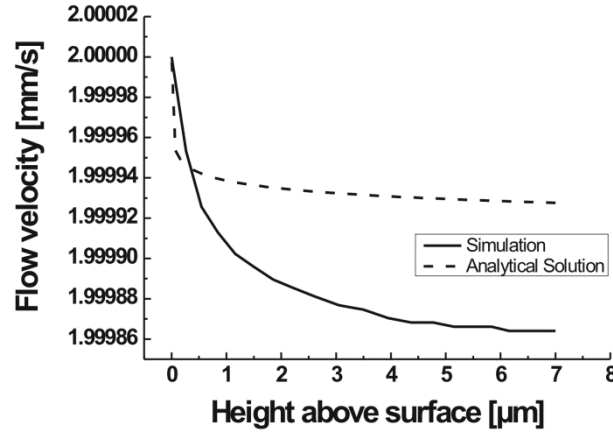


Figure 13: Comparison between numerical and analytical solution of mucus flow velocity depending on the height above the surface (interface between PCL and mucus).

5.4.1.2 Particle Velocity and Path Inside Mucus

In the following section, the velocity and the path of a particle inside the mucus flow after deposition is described. Under the assumption of a laminar flow, the drag force for a spherical particle can be written according to the Stokes law:

$$F_r = 6\pi\mu_M V_{rel} r \quad (11)$$

with μ_M = viscosity of the mucus, r = particle radius and V_{rel} = relative velocity between particle and fluid flow. To consider the vertical movement of particles (in z -direction, orthogonal to mucus flow), we released a particle into the mucus with some initial velocity W_0 in z -direction. The particle motion is essentially determined by the balance of inertia force and drag force. As there is no flow in z -direction now, the equation of motion was given by

$$m_P \dot{W} = -6\pi\mu_m W r + f \quad (12)$$

where m_P is the particle mass. Here, f represents constant forces like gravitation and buoyant forces. The solution of this (ordinary differential) equation was

$$W(t) = W_0 \exp\left(-\frac{9\mu_M}{2\rho_P r^2} t\right) + \frac{f}{6\pi\mu_M r} \quad (13)$$

where ρ_P is the density of the particle. To estimate the behavior of the velocity $V(t)$, relevant values, for instance, $\rho_P = 1125 \text{ kg/m}^3$, $r = 100 \times 10^{-9} \text{ m}$ were considered. Mucus viscosity $\mu_M(z)$ was modeled as linearly increasing from 1 mPas at the bottom to 6 Pas at the mucus/air interface. As particles do not move much in z -direction, this can be approximated by using the constant value of 6 Pas at the air interface. Buoyant forces and gravitation forces result in values in the order of the size 10^{-17} N , whereas friction force is about 10^{-11} N for a typical mucus velocity of 2 mm/min. Thus, buoyant forces and gravitation force could be neglected compared to the friction force. Looking on the particle velocity, after $t = 1.9 \times 10^{-12} \text{ s}$ the initial velocity has decreased to approximately 1 % of its original value. In addition, horizontal velocity (x -direction, parallel mucus flow) could be considered. The equation of motion was given by

$$m_P \dot{U} = -6\pi\mu_m(v - u_f)r + f \quad (14)$$

where u_f is the flow velocity of the mucus (depends on z). Approximating that the particle does not move much in vertical direction it could be assumed that the particle is located in a constant height, hence, the fluid flow velocity at particle position is constant ($u_f = u_0 =$ mucus drive velocity) which is feasible by looking at the only slightly decreasing flow velocity (figure 13, section 5.4.1.1). Using the equivalent equation of motion for the horizontal direction, the following solution could be obtained:

$$U(t) = u_f \left(1 - \exp\left(-\frac{9\mu_M}{2\rho_P r^2} t\right)\right) + \frac{f}{6\pi\mu_M r} \quad (15)$$

That means, the size of acceleration of a particle is the same as the deceleration in vertical direction. Hence, the particle immediately accelerates to flow velocity. Now, the particle path could be computed. In our case (with $f = 0$) the following equations could be obtained:

$$x(t) = u_f \left(t + \frac{1}{\alpha} \exp(-\alpha t) \right) + x_0 \quad (16a)$$

$$z(t) = -\frac{W_0}{\alpha} \exp(-\alpha t) + z_0 \quad (16b)$$

$$\alpha = \frac{9\mu_M}{2\rho_P r^2} \quad (16c)$$

In summary, particles deposited at the mucus air interface ($t = 0$) immediately accelerate to mucus transport velocity and uniform motion. This behavior is displayed in figure 14. Fast, de facto immediate, acceleration of particles trapped inside the mucus blanket causes the particles to show linear horizontal transport without a visible lag time. Here, numerical and analytical solution are in very good agreement.

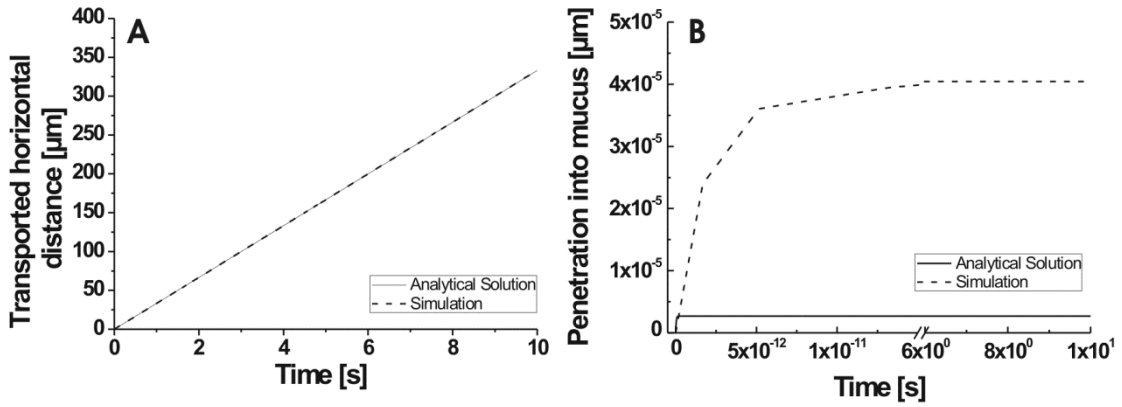


Figure 14: Vertical and horizontal particle transport upon deposition onto the the mucus layer. Particles are accelerated to horizontal mucus velocity by entrapment in the moving mucus layer which causes immediate horizontal transport. (A). Vertical particle velocity is decelerated immediately upon deposition to cause only slight penetration into mucus (B).

Regarding the vertical motion of deposited particles, inertia does not play a role in particle kinematics, as their vertical motion is decelerated close to zero even if particles impact with a velocity of 100 m/s perpendicular to the mucus blanket. This causes only slight penetration into mucus. Here analytical and numerical solution show some difference, as step size in the numerical solution leads to falsely increased penetration depth.

5.4.2 Simulation of Mucus Plasticity

Considering the presented results of particle mobility upon deposition, it could be shown that sedimentation of such particles within the mucus layer might not be a very probable mechanism for particle translocation across this layer. The question of possible further ways to access the underlying epithelium remains. One of those possibilities might be the displacement of particles by plastic deformation of the mucus slab itself or deposition on poorly covered patches of the epithelium. Here, on the one hand, the aim was to investigate if such mucus slabs are likely to retain their shape (i.e. retention of existing gaps within the mucus layer would also be possible) within physiologically relevant time spans (minutes to hours, the time needed to clear particles from the lungs). On the other hand plasticity of mucus slabs was analyzed to investigate whether particles deposited on top could access the epithelium by deformation of mucus slabs involving mass transport from top to bottom. Therefore, numerical grid-free methods (FPM) were applied which could simulate the plasticity of 2D mucus slabs of a given cuboid shape upon removal of restraining boundaries at the sides of the slab. These simulations gave insight into the time frame of deformation of mucus slabs and the velocity and direction of deformation by gravitational forces and diffusion. It was shown that mucus slabs can be considered rather stable in terms of deformation within physiologically relevant time spans: Figure 15 shows mucus slab deformation within a time span of 800 s. Here, figure 15A and 15B display the initial situation ($t = 0$), figure 15C and 15D represent mucus deformation after 400 s. Figure 15E and 15F display mucus deformation after 800 s.

Within this time, the cuboid mucus slab decreases in height by approximately 40 %. Similarly, the slab flattens out and increases in surface. It can be shown that the magnitude of deformation velocity of mucus is greatest in the area of the upper edges whereas mucus in the area of the center of the slab shows smallest flow velocities. Concerning the magnitude of the horizontal mucus deformation velocity (u_x , figure 15B, 15D, 15F), it could be shown that, again, areas of greatest velocity are located on the upper edges of the cuboid mucus slab. In summary, it can be concluded that the shape of such mucus slabs will be maintained within time spans of physiological relevance, where areas of greatest deformation and flow velocity are located on the upper edges of the mucus slab.

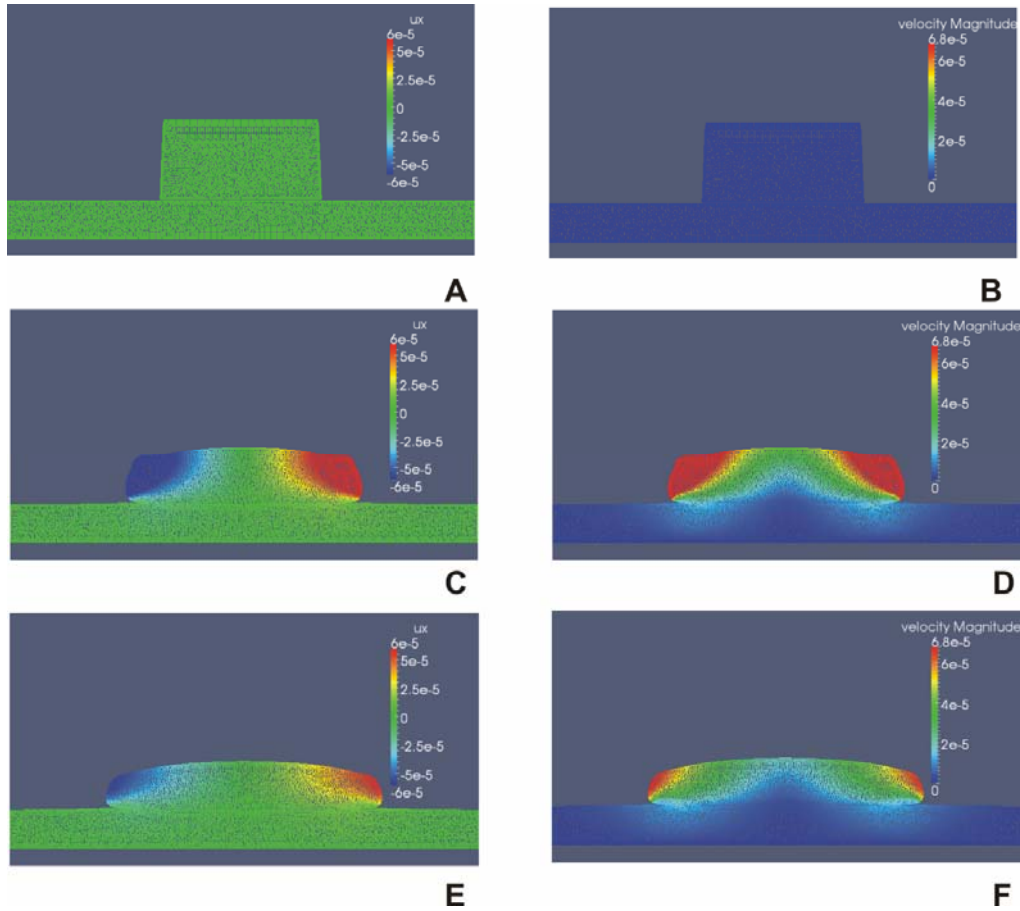


Figure 15: Deformation of cuboid mucus slab by gravitational forces and diffusion after 0 s (A+B), 400 s (C+ D) and 800 s (E+F). Images on the left (A, C, E) show magnitude of horizontal deformation velocity whereas images on the right (B, D, F) represent magnitude of total deformation velocity. Dimension of all data is m/s.

5.5 Discussion

5.5.1 Particle Trajectories

The aim of this study was to describe the mobility of nanoparticles in a complex biological fluid such as respiratory mucus and the interactions of such particles with this fluid. Particle trajectories and mobility of inhaled particles during impaction and sedimentation within mucus and mucociliary clearance were solved numerically and analytically. In addition, mucus plasticity was numerically solved to investigate further possibilities for particle translocation across the mucus layer. Analytical and numerical considerations of

particles trajectories deposited onto mucus showed that inertia does not play a significant role in the movement of particles within mucus. It could be shown analytically as well as by simulation that particles which are deposited at the air-mucus interface immediately accelerate to the velocity of the moving mucus layer. Vertical motion of particles during deposition could also be solved numerically and analytically: Immediately upon deposition, vertical particle velocity is decelerated quickly close to zero i.e. particles do not penetrate significantly inside the mucus layer. Here, impaction velocity only plays a marginal role in the quantitative behavior of particle sedimentation. Although simulations were in good accordance with the analytical solution, slight differences were visible. These were most probably due to step size during simulation. However, all these findings are in accordance with previous experimental studies and simulations concerning mucus flow, even for models involving much more complex mathematical description of mucus propulsion by ciliated cells (Barton and Raynor, 1967; Fulford and Blake, 1986; Smith, Gaffney et al., 2007; Smith, Gaffney et al., 2008).

5.5.2 Mucus Plasticity

To assess further possibilities for nanoparticles to reach the underlying epithelium, plasticity of mucus structures was studied: It could be shown that deformation of mucus slabs might be slow enough to allow retention of mucus structures within physiologically relevant time spans, i.e. before the structures are cleared by ciliary propulsion (minutes to hours). This finding is supported by previous experimental work which showed that the mucus layer is heterogeneous in height, appearance and surface coverage over the whole airways and does not form one continuous layer (Iravani and Melville, 1976; Im Hof, Gehr et al., 1997; Sims and Horne, 1997; Gehr, Im Hof et al., 2000). From this, one could conclude that possible gaps within the mucus layer might be retained in shape such that particles deposited there would have direct access to the underlying epithelium. Furthermore, it could be shown that during deformation the upper edges of the mucus slabs are deformed with greatest velocity. Particles deposited there might be transported towards the epithelium within the mucus. Clearly the presented approach represents only a rough approximation to the real situation, as interfacial physico-chemistry was not included in the model. Surface tension and other related effects cannot easily be modeled and need to be thoroughly assessed to completely mimic mucus spreading. In addition to that, further

studies concerning exact particle position in this situation and collision of two or more mucus slabs and its influence on deposited particles should follow. In summary, the question of particle translocation across the mucus layer can be addressed in the following way: The presented findings show that particles deposited on top of the mucus layer are very unlikely to cross this layer by sedimentation, diffusion or impaction, at least within time spans of physiological relevance, i.e. before particles entrapped by mucus are excreted by mucociliary clearance. However, deposition of particles in gaps within the mucus layer which were shown in our studies to retain their shape at least for short- and mid-term considerations, may be a possibility for particles to directly access the epithelium. Furthermore, deformation or collision mucus slabs may also lead to translocation of entrapped particles to the epithelium due to mass transport on the edges of the mucus slabs.

5.6 Conclusion

In this section the role of mucus fluid dynamics in the process of mucociliary clearance for the fate of deposited particles was investigated. Both numerical and analytical solutions to the problem were applied. Although using several approximations, it could be shown that the presented results were in accordance to previous studies with much more complex models. Both solutions were also in sufficient accordance to each other. In principle, the presented study displayed the kinematic behavior of deposited particles. One main conclusion from the presented results is the fact that particles cannot penetrate the mucus blanket by impaction or sedimentation alone and seem to be rather immobile once deposited onto the mucus blanket. This is a fact which is in accordance to the results described in the previous section: Here no difference in mucociliary clearance of several parameters was found. This is particularly feasible as there is no relative velocity between the particles and the moving mucus layer as suggested by the results presented here. However, particle mobility and diffusion on the microscale have to be considered to complete the understanding of particle fate within the mucus layer of the lungs. This is approached in the section to come.

6. The Role of Micro- and Macrostructure of Mucus in Particle Mobility

Parts of this chapter were published in:

Kirch, J., Schneider, A., et al. (2012). *Optical tweezers reveal relationship between microrheology and particle penetration of pulmonary mucus.* submitted for publication

The first author contributed the following points to the publication:

- design, performance and interpretation of experiments
- writing of the manuscript

The second author of the publication performed experiments involving optical tweezers.

6.1 Abstract

In this study the mobility of nanoparticles in mucus and similar hydrogels as model systems was assessed to elucidate the so far missing linkage between microscopic diffusion behavior and macroscopic penetration of such gels. Differences in particle adhesion to mucus components were strongly dependent on particle coating. Particles coated with 2 kDa PEG exhibited a decreased adhesion to mucus components whereas chitosan strongly increased the adhesion. In spite of such mucoinert properties of PEG, magnetic nanoparticles of both coatings did not penetrate through native respiratory mucus, resisting high magnetic forces even for several hours. However, model hydrogels were, indeed, penetrated by both particles in dependency of particle coating, obeying the theory of particle mobility in an external force field. Comparison of penetration data with cryo scanning electron microscopy (cryo-SEM) images of mucus and the applied model systems suggested particularly high rigidity of the mucin scaffold and a broad pore size distribution in mucus as reason for the observed particle immobilization. Active probing of the rigidity of mucus and model gels with optical tweezers was used for the first time within this context to confirm such properties of mucus on the microscale, thus presenting the missing linkage between micro- and macroscopical observations: Due to high heterogeneity in the size of the voids and pores of mucus, on small scales, particle mobility will depend on adhesive or inert properties. However, particle translocation over distances larger than a few microns is restricted by highly rigid structures within the mucus mesh.

6.2 Introduction

Mucus is a complex fluid of spatially varying properties containing hydrogel-forming glycoproteins (mucins) that enable the exchange of nutrients, provide lubrication, and protect the body from environmental influences. A compact layer of this hydrogel covers the complete gastrointestinal tract, the urogenital tract and the epithelium of the upper and central lung. Especially in pharmaceutical research, the barrier function of mucus is of special importance. Translocation of particulate matter such as dust, pathogens like viruses, or pharmaceutical (nano)carriers through this barrier is currently under investigation but

still not completely understood. In contrast to pathogens or toxic agents, penetration of this mucus barrier is strongly desired for any kind of drug delivery device, such as (nano)particulate application systems. Here, especially modification of particles with polyethyleneglycol (PEG) was reported to enhance particle diffusivity within the probed timeframe. On the contrary, chitosan is established as mucoadhesive, intending to increase bioavailability, but may thus decrease particle diffusivity.

In the last years, the investigation of the microrheology of mucus in this context has been gaining momentum (Lai, Wang et al., 2009). In particular the discrimination between different filtering effects, their correlation with gel structure and further details on how such filtering is controlled are being investigated (Lieleg and Ribbeck, 2011). Furthermore, the influence of electrolytes such as bile salts on particle mobility in mucus is tackled (Macierzanka, Rigby et al., 2011). The most established parameters to describe filtering effects are pore size (Sanders, De Smedt et al., 2000) and particle-mucus interactions (Mura, Hillaireau et al., 2011). The pore size is derived either from imaging data or particle tracking experiments. Particle tracking also provides information on mucociliary clearance and particle interactions with components of the mucus' polymer mesh (adhesion to mucins). Current studies in this field either focus on pore size as limiting factor (Olmsted, Padgett et al., 2001; Dawson, Wirtz et al., 2003) or suggest the more complex interaction filtering of mucus rather than size-exclusion effects (Lieleg and Ribbeck, 2011). Concerning non-cryo microscopic imaging, a disadvantage of such methods is their susceptibility to artifacts due to their harsh conditions, staining, or sputtering. Particle tracking experiments on the other hand suffer from limitations either in short correlation time, small observed area, or both. An alternative to such small-scale mobility of particles in mucus are classical diffusion chamber studies which quantify translocated particle fractions (Sanders, De Smedt et al., 2000). Those studies, however, do not provide information about microscopic particle behavior and mucus structure.

Therefore, although each being extensively investigated, the major problem in this field is the still missing linkage between penetration behavior on scales larger than a few micrometers and microrheology and -structure of mucus. The presented study bridges this gap through combination of advanced methods which, to our knowledge, have not been applied so far in this context. Initially, particle-mucus interactions were investigated by force spectroscopy to quantify adhesion of differently coated nanoparticles to mucus components to confirm muco-inert or mucoadhesive properties of the applied particles.

Penetration of such differently adhesive particles through mucus and model gels was investigated by quantifying penetration velocity of magnetic particles through capillaries filled with mucus or model gels. Penetration behavior was assessed considering the theory of particle mobility in a distinct force field. This macroscopic particle mobility was correlated to microscopic mucus rheology and structure. Here, cryo scanning electron microscopy (cryo-SEM) was applied which allowed for an unbiased determination of the native mucus structure. Furthermore, optical tweezers were used to passively and actively probe native respiratory mucus. This approach is unique in this context and demonstrated that one crucial point in particle mobility is not only the pore size distribution but also mucin scaffold rigidity which is not captured in regular methods to measure mucus microrheology. This combination of pore size and rigidity in mucus could be used to explain the mentioned discrepancy between micro- and macrorheology of mucus as well as between low long distance mucus penetration and previously observed microscopic particle mobility.

6.3 Experimental

6.3.1 Materials

All particles were obtained from commercial sources: For force measurements, PS particles with covalently linked coating (chitosan and polyethyleneglycol (PEG, 2 kDa), 500 nm diameter, Kisker Biotech, Steinfurt, Germany) were used. Capillary penetration experiments were conducted with dextran iron oxide composite particles with covalently linked coating (chitosan and PEG, 2 kDa) with a diameter of 170-200 nm (Micromod, Rostock, Germany). For the experiments with the optical tweezers, either polymethylmethacrylate (PMMA) beads (Fluka Productions GmbH, Buchs, Switzerland) with a size of 4 μm or melamine resin beads (Fluka Productions GmbH, Buchs, Switzerland) with a size of 5 μm were used. For optical tweezer experiments, the observation of the samples was done with a Gene Frame (ABgene, Epsom, United Kingdom), a special sample cell with a low volume of 25 μl . All chemicals used were of analytical grade and purchased from standard commercial sources. Nanoparticles were characterized regarding their size distribution by nanoparticle tracking analysis (NTA).

Measurements were performed with a LM10-HS (NanoSight, Amesbury, United Kingdom). This technique was previously demonstrated to be more precise in determining particle size distributions than standard dynamic light scattering (DLS) especially for polydisperse samples (Filipe, Hawe et al., 2010). Particle size distribution is displayed below (figure 16).

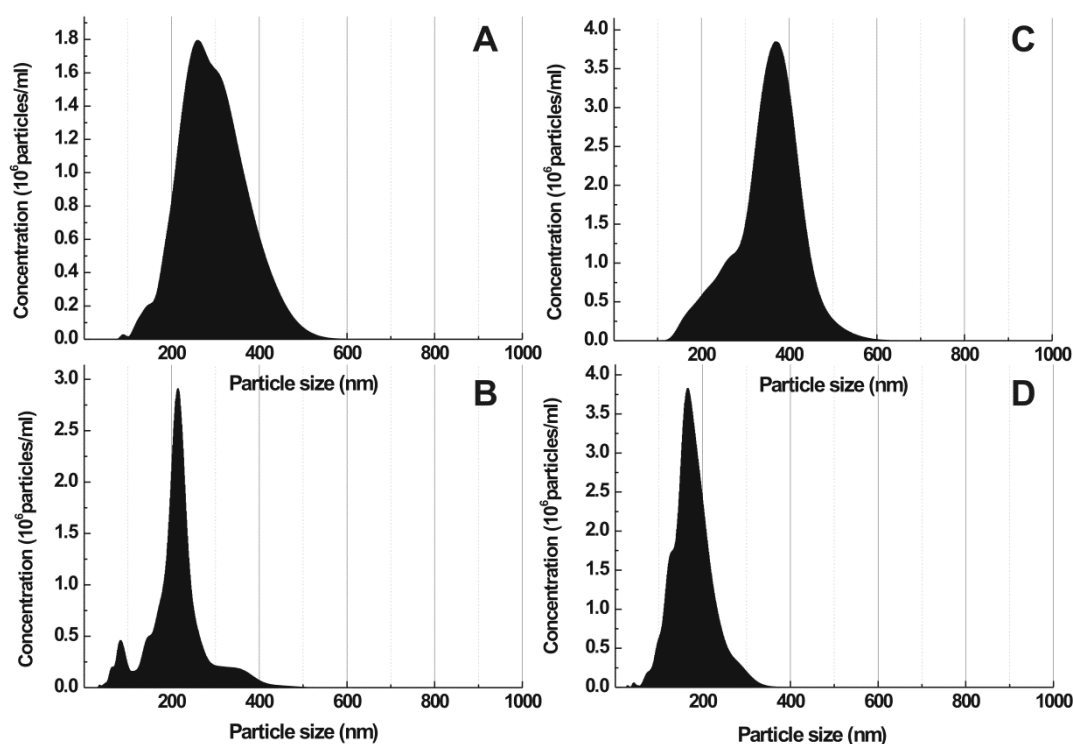


Figure 16: Particle size distribution (hydrodynamic diameter) of PS particles (A+C) and magnetic dextran particles (B+D) with PEG 2 kDa coating (right) or chitosan coating (left). Size distribution is averaged over $n = 3$ independent experiments.

6.3.2 Atomic Force Microscopy

AFM cantilevers were cleaned and modified according to a previously described procedure (Gfeller, Nugaeva et al., 2005). In short, cantilevers were cleaned twice in piranha etch (97 % H_2SO_4 in 30% H_2O_2 ; 1:1), rinsed in millipore water and dried under nitrogen flow. Cantilevers were suspended in silane solution (1 % 3-glycidyloxypropyl-trimethoxysilane,

0.5 % N-ethyl-diisopropylamine in water-free toluene) for 4 h at room temperature to form a self-assembled monolayer (SAM), providing a hydroxyl-reactive surface towards primary hydroxyl groups of mucins. After silanization, cantilevers were rinsed twice for 20 min with dry toluene and dried under nitrogen flow. Subsequently, cantilevers were suspended overnight in 1 % mucin solution followed by a rinsing with millipore water. The sample substrate was silica, cleaned equally as the used cantilevers. A drop of particle suspension (chitosan or 2 kDa PEG coated polystyrene particles respectively in millipore water) was placed onto the substrate and dried in air. These samples were used in subsequent force imaging. Samples were inserted into the fluid cell of the AFM (Multimode V, Bruker, Santa Barbara, USA). Measurements of force plots (force spectroscopy) were done via so-called force volume imaging in fluid conditions where a surface is scanned while recording force-distance plots for each pixel of the image (figure 17). Force volume images (4096 force plots per image) were taken of the samples with 10 nN trigger force and a surface dwell time of 1 s. Force plots attributed to the particles were extracted, analyzed and compared to the force plots attributed to the substrate with nanoscope 7.13 software (Bruker, Santa Barbara, USA). Adhesion force was averaged over all force plots attributed to one particle. Several particles ($n > 6$) were analyzed and the statistical variation in average adhesion force among the particles considered as statistical error.

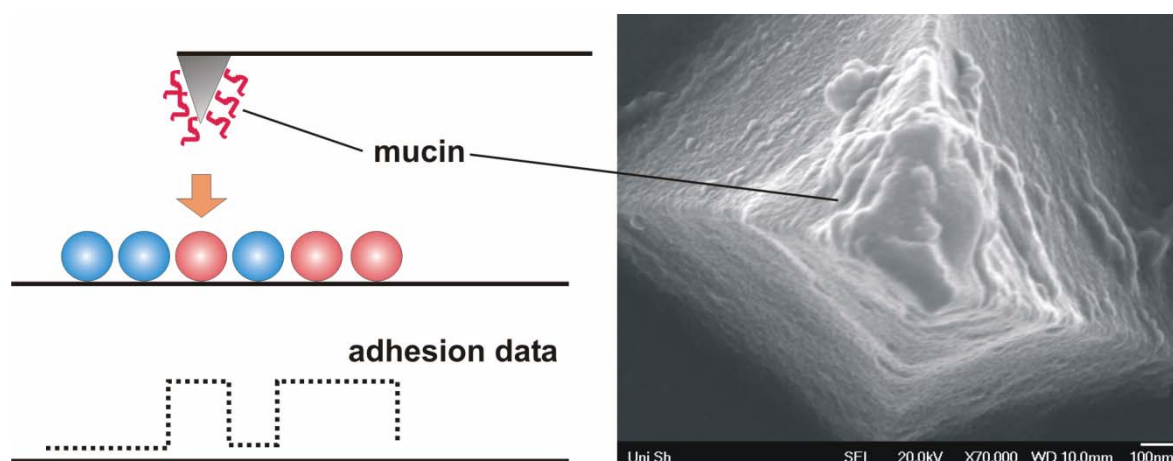


Figure 17: Force volume imaging allowed for the discrimination between mucoadhesive (red) and mucoinert particles (blue) by the magnitude of adhesion to the mucin functionalized cantilever tip (left). SEM images of the modified tip (right) display the dense layer of mucin on the tip.

6.3.3 Capillary Penetration Experiments

Capillary penetration experiments were conducted according to a method recently introduced by Kuhn et al. (Kuhn, Hallahan et al., 2006). Briefly, capillaries were filled with a model gel or respiratory mucus, respectively and sealed with vacuum grease on one end. 10 μl of particle suspensions (chitosan or 2 kDa PEG coated magnetic dextran iron oxide composite particles, Micromod, Rostock, Germany) were pipetted on top of the gel column. Filled capillaries were placed upright with their sealed end in a reproducible position in 2 mm distance to the pole of a neodymium magnet (figure 18). Capillaries were fixed in a reproducible position next to the pole of the magnet (neodymium permanent magnet).

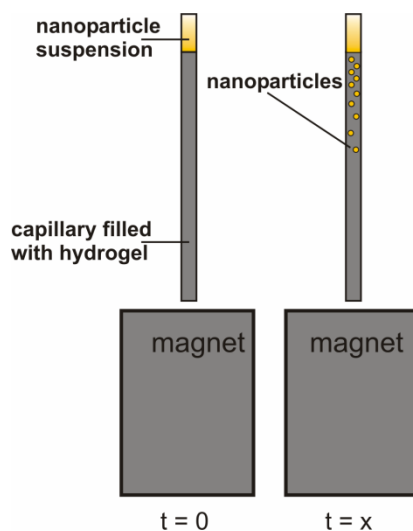


Figure 18: Gel filled columns were placed upright next to the magnet. Nanoparticle suspensions were filled on top of the gel columns. Magnetic particles were pulled through the hydrogel mesh upon exposure to the magnetic field.

A fit with the model of Chrumbach and Rodbard was done according to a procedure described previously (Sarbolouki, Mahnam et al., 2004). Here particle mobility in an external force field as described as function of gel concentration is given by

$$m = m_0 e^{-kc} \quad (17)$$

where m is the particle mobility, m_0 the mobility in water, c the polymer concentration, and k the system specific constant. Velocity of the magnetic particles while being pulled through model gels or mucus was obtained by measuring the travelling time of the particle at a fixed position in 2-4 mm distance to the pole of the magnet.

Native respiratory mucus was obtained during bronchoscopy of a healthy horse and stored at -80 °C. According to previous studies, storage should not influence mucus rheological properties (Gastaldi, Jardim et al., 2000). There was no access to mucus of further healthy individuals. Model gel was hydroxyl-ethyl-cellulose (HEC, SE Tylose GmbH & Co. KG, Wiesbaden, Germany) of various concentrations. To prepare model gels, the respective amount of HEC was dissolved under overnight stirring in millipore water.

6.3.4 Cryo-SEM

HEC hydrogels and native respiratory mucus were imaged by cryo-SEM. HEC gels were prepared by dissolving the respective amount of HEC in millipore water. Before SEM imaging, HEC gels and mucus were collected in a thin dialysis capillary. Gel-filled capillaries were immediately frozen in liquid propane, to only allow formation of amorphous- and circumvent formation of crystalline water. Capillaries were cut into smaller pieces to subsequently image the brim of the cut. Sublimation of frozen, amorphous water inside the porous HEC gel and mucus was carried out for 1 h at -100 °C (Baltec SCD 500 Sputter coater, Baltec/Leica, Germany). Subsequently, the surface of the dry polymer scaffold was sputter coated with platinum (layer thickness approximately 12 nm. After sputtering, samples were transferred into the SEM (DSM 982 Gemini, Zeiss, Jena, Germany) and imaged at -120 °C and 5 keV with 5-6 mm working distance.

6.3.5 Optical Tweezers

To probe the microstructure of the respective medium, the choice of the bead had to be adapted to the optical properties of the fluid. In 1 % HEC gel (refractive index ≈ 1.33) PMMA beads (refractive index ≈ 1.48) were used while in mucus melamin resin beads

(refractive index ≈ 1.68) proved to be the optimal choice. Here, the difference in refractive index should be maximized. For the preparation of the samples, a small volume of beads (2-4 μl) with a solid content 10 % was mixed with about 100 μl of the respective fluid. The concentration of beads was chosen in a range of 200-2000 ppm, so that hydrodynamic interactions between multiple beads could be neglected. Following the mixing process, all samples were vortexed for about five minutes to make sure that the beads were distributed homogeneously within the fluid. 25 μl of this mixture were filled into the sample holder and sealed airtight with cover glasses and vacuum grease.

The setup of the optical tweezers was identical with the one used by Ziehl et al. (Ziehl, Bammert et al., 2009). The beam of a solid state laser (Ciel, Laser Quantum, Cheshire, United Kingdom) was guided towards the oil immersion objective (numerical aperture = 1.4, 60 x magnification) to create a harmonical trapping potential within its focal region inside an inverted microscope (Eclipse TE2000-S, Nikon GmbH, Duesseldorf, Germany). The visualization of trapped beads was achieved by illuminating the sample with an LED illumination source (ZLED CLS 9000, Zett Optics, Braunschweig, Germany) from above in the inverse direction of the laser beam through the sample cell onto the chip of a high speed camera (HiSpec 2G, Fastec Imaging, San Diego, CA, USA). The beads were recorded for a duration of 16 s with a sample rate of 16 kHz and tracked afterwards by the means of a cross correlation algorithm realized in LabView 2011 (National Instruments Germany GmbH, Munich, Germany) which allowed for the determination of the particle displacements with a spatial resolution of approximately 2 nm (Cheezum, Walker et al., 2001).

Two types of measurements were conducted: In passive tracking experiments, a bead was held in place by the trap and the Brownian motion was recorded as reported above. Active experiments were performed by moving the piezoelectric stage of the setup in a triangular oscillation pattern induced by the signal of a waveform generator. The amplitude and frequency of the oscillation were chosen according to the mobility of the bead at its current position (usually between 1 μm and 4 μm and respectively 0.1 Hz and 0.2 Hz). The observation time was chosen in a way that at least two full oscillation periods could be recorded. Synchronous to image acquisition the voltage signal driving the stage was recorded by a data acquisition card (National Instruments Germany GmbH, Munich, Germany). All optical tweezers measurements were performed at a temperature of 20 °C.

6.3.5.1 Determination of the Shear Moduli

The shear moduli were determined from the displacement data of beads that were confined in the focal region of the optical trap. This was achieved for mucus as well as for the HEC model gel by a method proposed in 1997 by Schnurr et al. (Schnurr, Gittes et al., 1997) according to which the Fourier-transformed displacements (\tilde{x}) are linked to the force spectrum of Brownian motion (\tilde{F}) by a response function $\tilde{\alpha}$, the compliance, which is a complex function of the frequency ω for non-Newtonian fluids.

$$\tilde{x} = \tilde{\alpha}^* (\omega) \tilde{F}_r \quad (18)$$

Here, Fourier-transformed quantities are denoted by a tilde and the compliance is given by

$$\tilde{\alpha}^* (\omega) = \alpha' (\omega) + i\alpha'' (\omega) \quad (19)$$

while the power spectral density (PSD, $\langle |\tilde{x}(\omega)|^2 \rangle$) of the particle displacements can be related directly to the imaginary part of the response function α'' by applying the fluctuation-dissipation-theorem (Landau and Lifshitz, 1966). The parameter α' can be obtained by applying the Kramers-Kronig-relations as previously demonstrated (Addas, Schmidt et al., 2004):

$$\langle |\tilde{x}(\omega)|^2 \rangle = \frac{2k_B T}{\omega} \alpha''(\omega) \quad (20a)$$

$$\alpha'(\omega) = \frac{2}{\pi} \int_0^\infty \frac{\zeta \alpha''(\zeta) - \omega \alpha''(\omega)}{\zeta^2 - \omega^2} d\zeta \quad (20b)$$

The connection between the compliance of the material and its shear modulus is finally given by

$$G^* (\omega) = \frac{1}{6\pi R} \cdot \frac{1}{\tilde{\alpha}^* (\omega)} \quad (21)$$

where the shear modulus is given as

$$G^*(\omega) = G'(\omega) + iG''(\omega). \quad (22)$$

At this point knowledge of the strength k of the optical trap is required because it influences the elastic properties of the fluid over the whole frequency regime in form of an additive constant:

$$G'_{\text{trap}} = k/6\pi R. \quad (23)$$

In the case of the HEC model gel these were determined directly out of the passive measurements by using the equipartition of energy relating the thermal energy with the harmonic trapping potential (Simmons, Finer et al., 1996). Due to the strong confinement of the polymer network however this was not possible in mucus. Instead the calibration of the trap strength was performed within a second sample cell containing water. The typical strength of the optical trap used in the experiment ranged between 3 pN/ μm and 8 pN/ μm . The frequency at which the corresponding apparent elastic modulus was reached also defined the lower data cut-off, typically around 1 Hz. The shear modulus at even lower frequencies would only represent the characteristics of the trap instead of those of the fluids. As upper cut-off, a frequency of 3.5 kHz was chosen which lies well below the Nyquist frequency (Shannon, 1949) of in our case 8.192 kHz. This choice was motivated by the minimization of aliasing errors.

6.4 Results

6.4.1 Force Spectroscopy

Determination of adhesive interactions between mucin fibers and nanoparticles of different surface chemistry could be realized by force spectroscopy. Direct comparison of adhesion forces between nanoparticles and silica substrate allowed for an unbiased comparison between chitosan and PEG (2 kDa) coated PS-nanoparticles. Relative adhesion compared to the substrate as shown in figure 19 demonstrated that chitosan coated particles adhered much stronger to mucin fibers attached to the tip of the cantilever than PEG coated particles. Whereas adhesion force between mucin functionalized tip and chitosan coated particles was over 250 % stronger than to the substrate, PEG coating of nanoparticles even resulted in a reduced adhesion compared to the bare silica substrate.

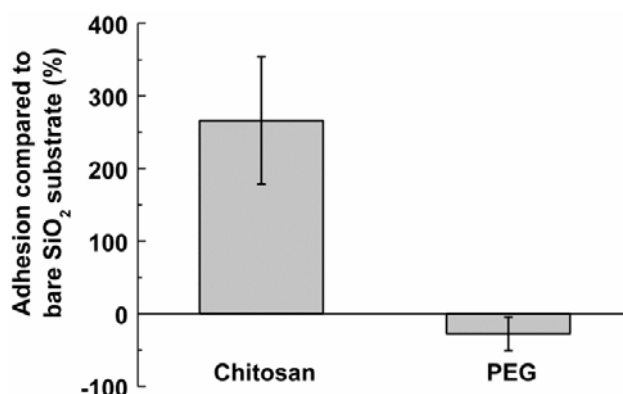


Figure 19: Adhesion of differently coated nanoparticles to mucin fibers compared to underlying silica substrate. Data shown as mean \pm SD.

6.4.2 Capillary Experiments

Penetration of magnetic particles over macroscopic distances in mucus and model gels was investigated by the method of Kuhn et al. (Kuhn, Hallahan et al., 2006). This method allowed for the analysis of direct translocation and penetration behavior of differently coated magnetic nanoparticles over defined distances in mucus and model systems. Investigation of penetration behavior over such distances may predict the potential of

particles to translocate through thick physiological mucus barriers rather than other methods.

To show the feasibility of the method and to perform a proof-of-principle, capillary experiments were conducted with HEC gels as a model system. Here, gradual transition from water to dense hydrogels was realized by applying HEC gels of gradually increasing concentration and thus also gradually increasing viscosity and elasticity. Penetration experiments were conducted with both types of particles (chitosan coating as well as PEGylated nanoparticles) which penetrated HEC gels allowing for the calculation of penetration velocities (figure 20).

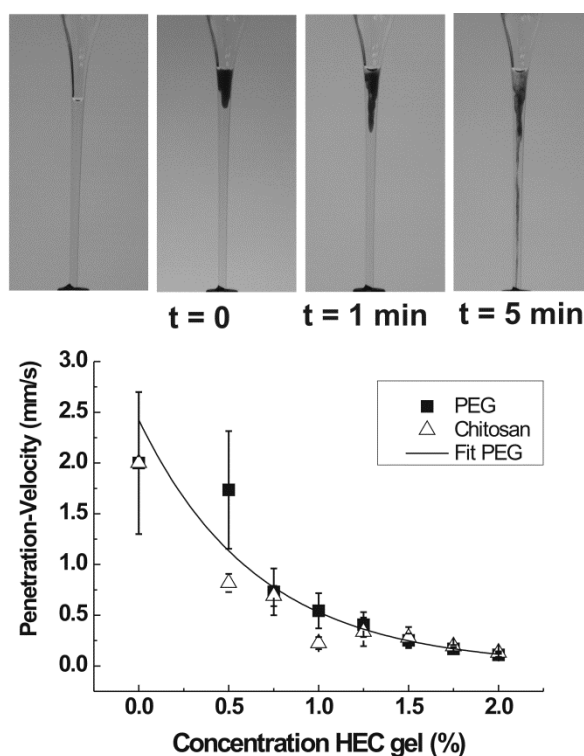


Figure 20: Penetration of PEGylated and chitosan coated magnetic nanoparticles through 1% HEC gel within 5 minutes (top). Penetration velocity was inversely related to gel viscosity and thus polymer concentration which could be fitted with the Chrombach-Rodbard model ($R^2_{\text{PEG}} = 0.93$). Adhesion of chitosan coated particles to cellulose fibers can be confirmed by drop in penetration velocity (bottom). Data shown as mean \pm SD, $n \geq 3$.

It was shown that penetration velocity was indeed strongly dependent on rheological properties and polymer concentration of the model gel (figure 20, bottom): Penetration velocities of the particles in the HEC gel of the highest concentration decreased to approximately a tenth of their initial value as measured in millipore water. Correlation of particle velocity with polymer concentration of the respective hydrogel can be used to assess the accordance of penetration behavior with theoretical models describing particle mobility in a force field. Fitting of penetration velocities with the model of Chrambach and Rodbard (Chrambach and Rodbard, 1971; Sarbolouki, Mahnam et al., 2004) shows that in general, sufficient congruence can be reached for the penetration behavior of PEG particles ($R^2_{\text{PEG}} = 0.93$) which exhibits greater conformity with the mentioned model than penetration behavior of chitosan coated nanoparticles: Here a fit with sufficient goodness could not be achieved. Performing the same experiments with native respiratory mucus, it could be shown that mucus is indeed a “tenacious fluid” (Florey, 1962): No penetration into, let alone through the mucus column could be observed (figure 21). This was true even for very long exposure (> 3 h) to the magnetic field. A difference between chitosan coated or PEGylated nanoparticles in this behavior could at no point be observed.

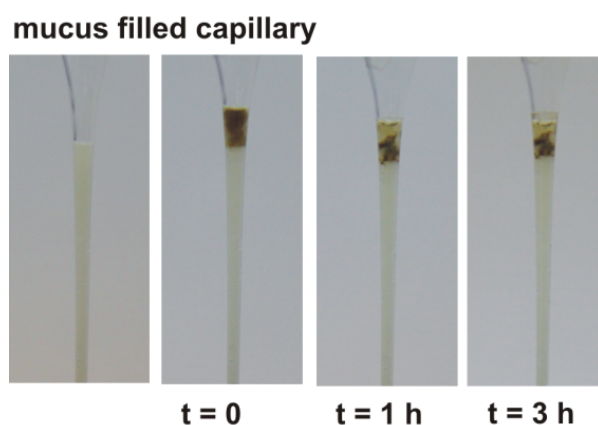


Figure 21: Magnetic PEG coated nanoparticles did not penetrate into a mucus filled column even within incubation times longer than 3 h.

6.4.3 Cryo-SEM

Structural analysis of mucus and HEC gels was performed with cryo-SEM. The structure of the polymer matrix of mucus and the differently concentrated HEC gels could be imaged in their native state. The porous polymer scaffold of the gels could be visualized with high resolution (figure 22-25). Pore size could be determined to range between approximately 100 nm to 500 nm in HEC of 0.5 % concentration (figure 22). With increasing polymer concentration, HEC hydrogels exhibit decreasing pore sizes as the polymer mesh becomes more condensed (figure 23). The average thickness of the fibers of the polymer scaffold can be determined to approximately 20 nm. Cryo-SEM imaging of mucus gel revealed a very different structure of the mucin polymer mesh: In mucus, large pores are heterogeneously combined with very small pores. Pore sizes of mucus ranged between approximately 100 nm and voids of several micrometers in diameter (figure 24). Furthermore, the thickness of the fibers of the polymer scaffold could be determined to be much higher than in HEC gels (figure 25).

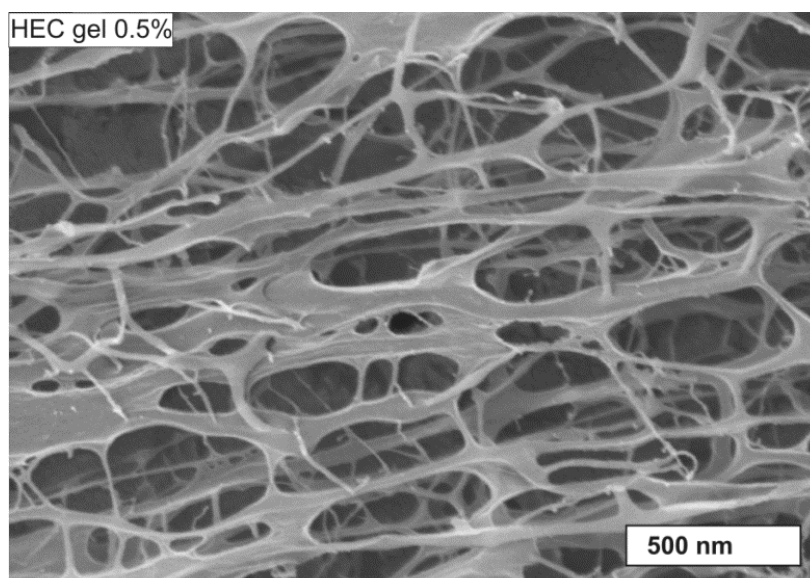


Figure 22: HEC gels of low concentration exhibit a very airy mesh structure with thin polymer fibers and large, quite homogeneous pore sizes.

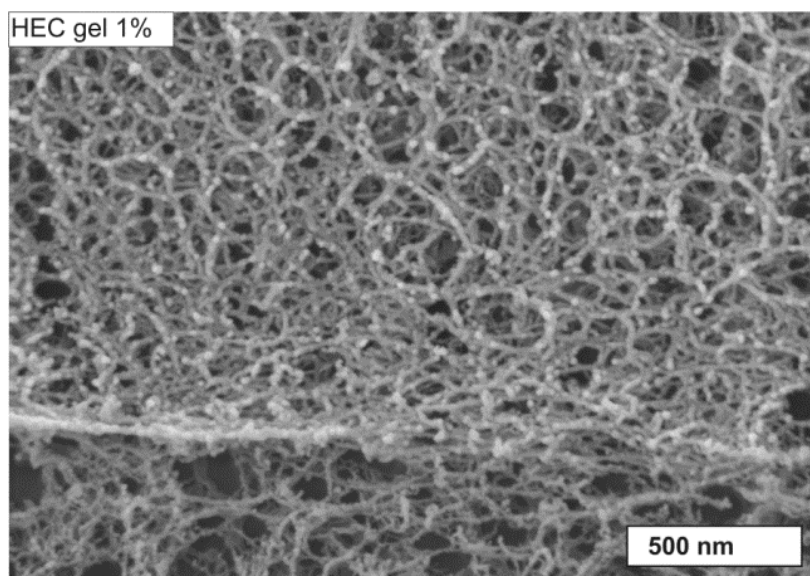


Figure 23: With increasing polymer concentration, the mesh of HEC hydrogel becomes more condensed and the sizes of the pores become smaller.

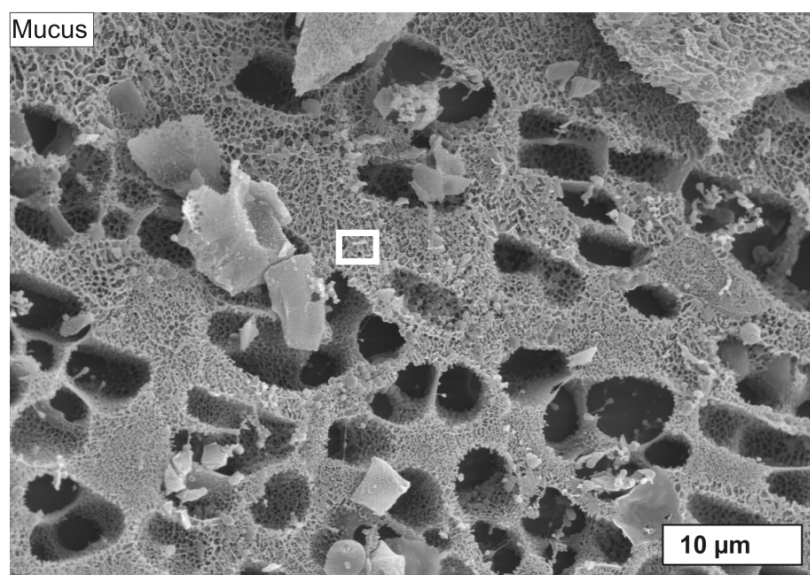


Figure 24: Mucus exhibits a very heterogeneous structure with a very broad pore size distribution from voids of several micrometers to small pores below 100 nm. The area marked with a white square is displayed in figure 25.

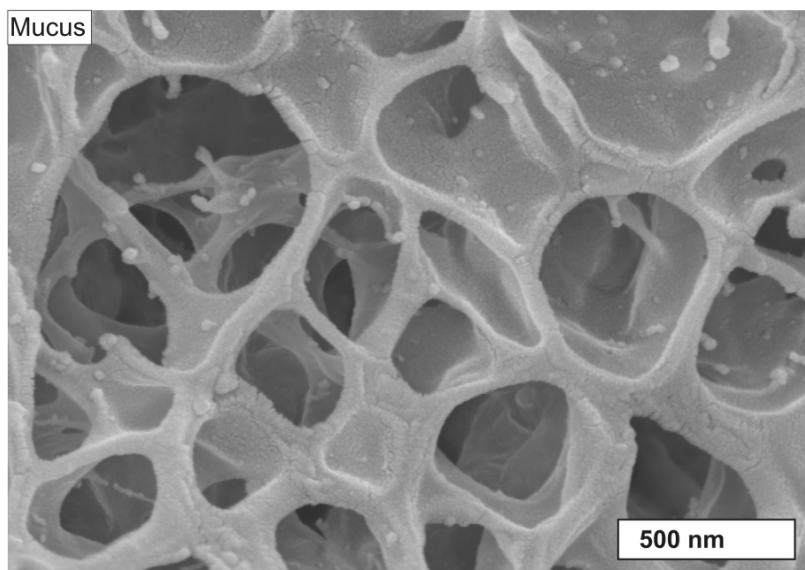


Figure 25: Polymer fibers in mucus are much thicker than in HEC hydrogels and form very thick pore walls, suggesting a high rigidity of the polymer mesh. Pores can be very small and do not seem to be very well connected.

6.4.4 Optical Tweezers

Optical tweezers as a non-invasive tool were applied to probe the microrheology and particularly the rigidity of the polymer scaffold on the micrometer scale. Here, native respiratory mucus as well as HEC model gels were analyzed in this regard with stationary and oscillating optical traps. In the case of the stationary, passive tracking experiment, a single bead was confined to a small spacial volume and the displacement from the center of the trap was recorded. Afterwards the MSD was calculated (figure 26 & 27). It is linked to the diffusion coefficient D of a fluid by the generalized Stokes-Einstein-equation (equation 3). In the case of a simple Newtonian fluid which does not show any elastic behavior, the coefficient α is equal to 1 and the MSD increases linearly with time. In contrast, for complex fluids like hydrogels the history of former deformations plays an important role on its flow properties and α may become bigger (superdiffusive behavior) or smaller than 1 (subdiffusive behavior). The one-dimensional MSD of the beads out of the center of the optical trap in dependency of the correlation time t of mucus (figure 26) and the HEC model gel (figure 27) is displayed below.

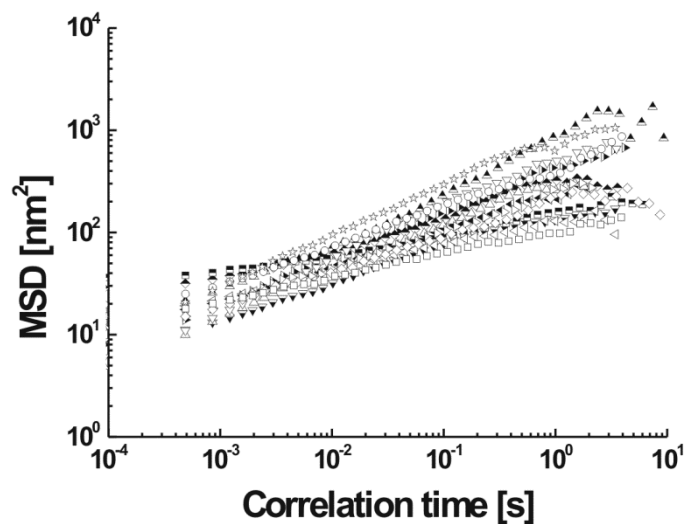


Figure 26: MSD values of the applied microparticles measured in native pulmonary mucus. Large range in the slope of the MSD values determines strongly heterogeneous, locally varying rheological properties. Symbols refer to different samples and different sites within the sample ($n_{\text{samples}} \geq 3$).

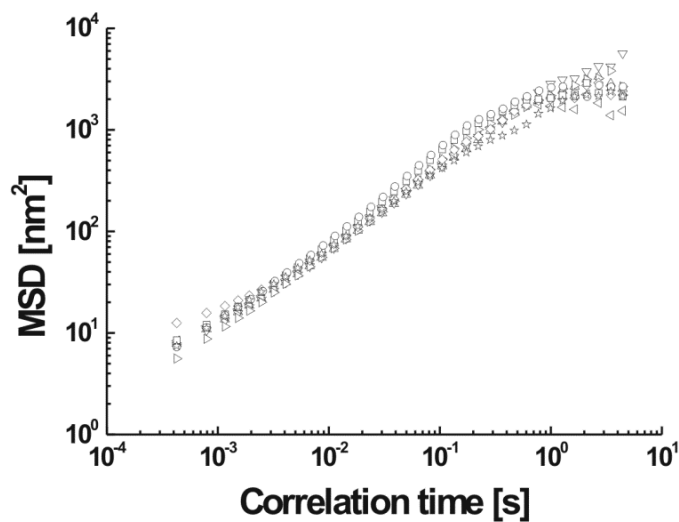


Figure 27: MSD values of the applied microparticles measured in HEC hydrogel (1 %). MSD values do not depend on site as observable by the highly homogeneous slopes. Symbols refer to different samples and different sites within the sample ($n_{\text{samples}} \geq 3$).

The data cut-off for long times was chosen at the point where the MSD reached a plateau defined by the constrictions either due to the optical trap or the polymer scaffold. Extensive heterogeneity of mucus morphology as suggested by cryo-SEM studies could be confirmed: Highly diverse slopes of the MSD of particles in mucus in dependence of correlation time indicate strongly varying local properties. Consequently, the observed range in absolute values suggests a large variety in particle mobilities that spans more than an order of magnitude at all observable correlation times. On the contrary, for HEC (1 %) the measured MSD values lay within a much smaller range, thus demonstrating a high rheological homogeneity of the bulk hydrogel.

Calculating storage and loss moduli, it was found that the microrheology of mucus presents itself much more diverse than that of HEC. While the mean range of the storage modulus in mucus (figure 28A) covered a whole order of magnitude at each frequency over the whole frequency regime, the fluctuations in HEC (figure 28C) were a lot narrower and typically did not move further apart than a factor of 2. The only exception were the moduli at lower frequencies than 20 Hz which showed a significant scatter which may be due to thermal drift of the piezo stage. Similar information could be deducted from the loss moduli (figure 28B and 28D), where, again, the range in mucus is even more significant.

In general the presented results imply a similar elastic as well as viscous behavior of mucus and HEC at frequencies between 10 Hz and 1000 Hz, differing mainly in terms of high material heterogeneity in mucus and high homogeneity in HEC gels respectively.

In the HEC model gel, material homogeneity could be recovered not only from the uniformity of the MSDs at different locations within the gel but also when considering displacements at a certain spot in different directions i.e. along the x - and y -axis of the pictures taken by the high-speed camera (figure 29). As displayed in figure 29B both curves overlap almost completely. On the contrary, in mucus strong deviations in the behavior of the MSD could be seen when comparing the x - and the y -direction of the trajectories (figure 29A). When comparing the values of the MSD along the y -axis at 0.35 ms and 1 s, there is only an increase by a factor of 3.25 while along the x -axis the values increase much steeper by a factor of 10.

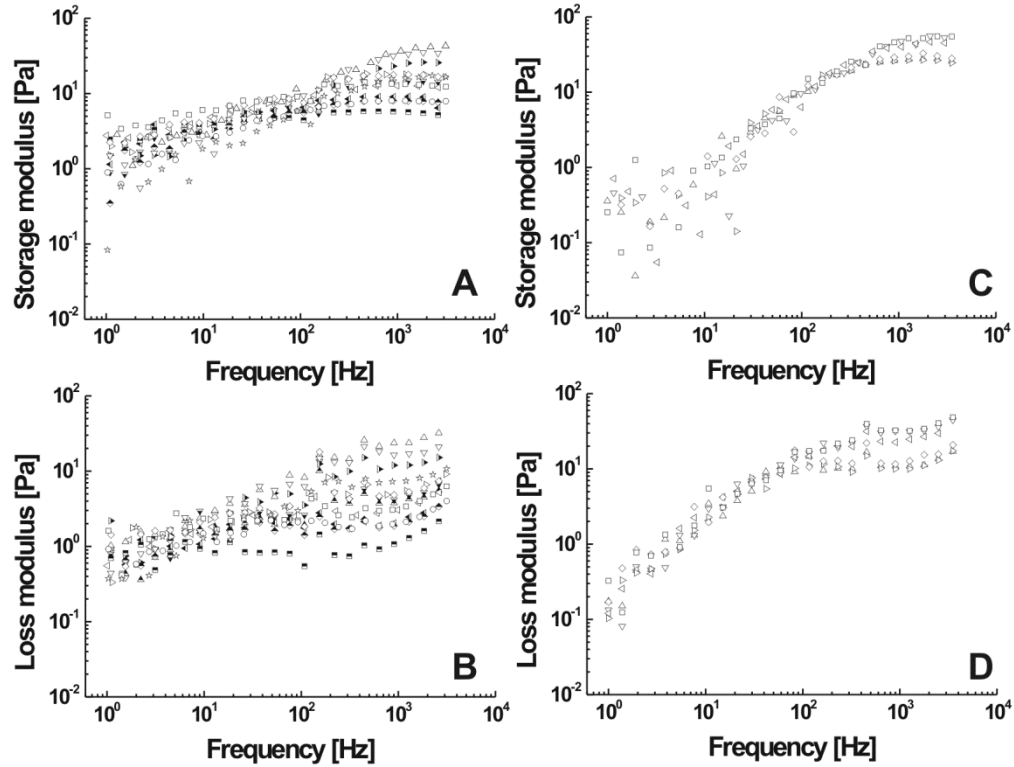


Figure 28: Storage- and loss moduli of mucus and HEC gel. Similar to MSD data, mucus (A+B) exhibits broad ranges of loss- and storage moduli. Contrary, HEC hydrogel shows homogeneous distribution of both moduli (C+D). Symbols refer to different samples and different sites within the sample ($n_{\text{samples}} \geq 3$).

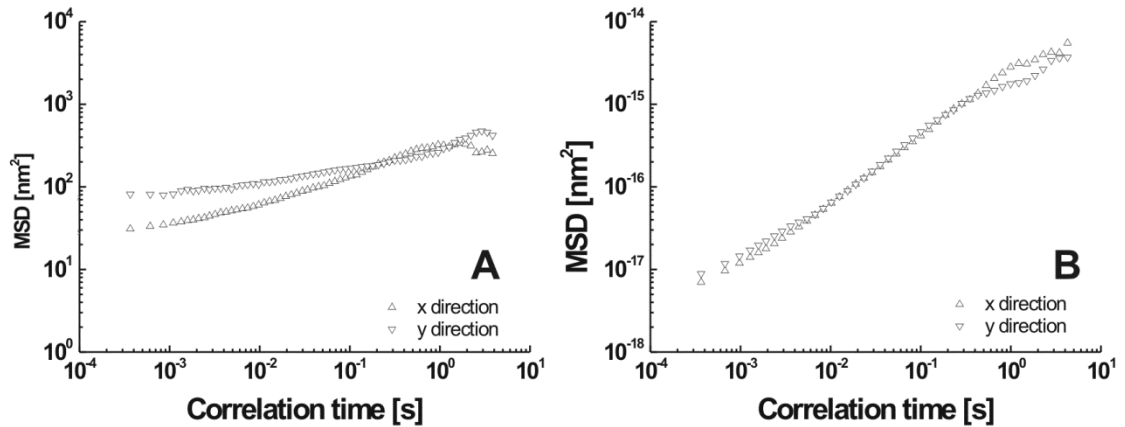


Figure 29: Material homogeneity is additionally displayed by comparing MSD data for x - and y -direction for mucus (A) and HEC gel (B). In mucus, both curves differ significantly demonstrating high material anisotropy whereas for HEC gels, both curves align well, demonstrating isotropic behavior.

Importantly, although suggesting quite similar microrheology for both systems (either the MSDs or the shear moduli), the clear difference in material homogeneity between mucus and HEC gel is in accordance with the completely different macroscopic penetration behavior of particles in mucus and HEC. Yet, according to the fluctuation data, both materials should react similarly at least on a microscopic scale. To grasp these seemingly contradictory properties, additional, active experiments had to be performed: Here, a bead was caught in the trap and the piezoelectric stage the probe cell rested on was moved in a triangular wave pattern. The motion of the stage and the displacements of the bead relatively to the center of the trap were recorded. It could be shown that trapped particles can easily be moved through the HEC gel (1 %) as the particle followed the moving trap (figure 30B), i.e. the force exerted on it by the laser was sufficient to distort, stretch, or even rupture the polymer scaffold of the dense HEC gel. On the contrary, active measurements within mucus (figure 30A) showed that most beads could not be moved significantly, demonstrating the high rigidity of the polymer scaffold.

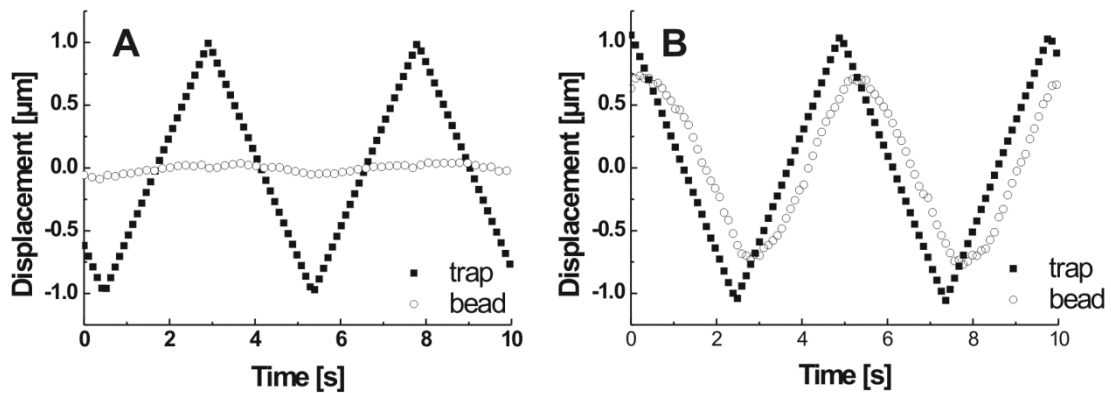


Figure 30: Active measurements by oscillating trapped beads reveals rigidity of the mucus mesh as trapped beads cannot be moved within the mesh while the trap is displaced by 1 μm in each direction (A). In HEC gel (B) the trapped bead follows the trap during the complete oscillation cycle.

6.5 Discussion

6.5.1 Force Spectroscopy

So far adhesive interactions between mucin fibers and differently coated nanoparticles were usually investigated via quantification of mucin adsorption to these particles. In such studies (Yoncheva, Lizarraga et al., 2005), PEGylation was shown to reduce mucin adsorption and thus adhesion. The presented results are in good agreement with those studies as increased adhesion with chitosan coating and decreased adhesion by PEGylation could be confirmed. However, the approach presented here has the advantage of comparing both types of particles directly with the underlying substrate as intrinsic control. Thus, the results presented here are independent on the used cantilever and its tip geometry which greatly influences adhesion data and has so far been an unsolved problem in the methodology of force spectroscopy. While PEGylation of particles to decrease adhesive interactions with mucus or mucins is a quite recent approach, application of chitosan coating to increase such interactions has been widely accepted (Smart, 2005). Thus, the influence of such different coatings on particle mobility in mucus of various sources has been accessed by different methods. However, as mentioned before, those methods suffer from several limitations. Therefore we applied a just recently developed method to probe long-distance/long-term particle mobility to increase to proximity to the *in vivo* situation. Here, particle mobility in mucus is investigated for time scales and spatial distances of higher physiological relevance as presented in section 6.4.2.

6.5.2 Capillary Experiments

The observed behavior was in accordance with theoretical description of the particle penetration through gels: The applied model describes penetration of spherical particles through hydrogels by application of an external force field (e.g. electrostatic or magnetic forces). The fact that this model incorporates inert i.e. non-adhesive particles as boundary condition may be the reason for the greater goodness of the fit for PEGylated particles: Similar to their interaction with mucins, chitosan coated particles may interact adhesively with HEC fibers. As HEC fibers are polysaccharides, chemical similarities to polysaccharide side chains of mucins over large areas cannot be doubted. Thus, HEC gels

might mimic mucus gel and its adhesion to chitosan or chitosan coated particles. This adhesive interaction is supposed to be largely due to electrostatic interactions (Andrews, Lavery et al., 2009).

Furthermore, the model of Chrmbach and Rodbard allowed for an estimation of the average pore size of the gel: According to this model, the pore size equals the size of the probe particles when penetration velocity drops to 50 % of its initial value. Considering the fit of penetration velocity of PEGylated particles, this means that the average pore size of HEC gels should be approximately 200 nm for concentrations around 0.5 % which could later be confirmed by cryo-SEM images of HEC hydrogels (section 6.4.3).

The fact that both types of particle did show penetration through HEC gels but not through mucus indicated the need to further characterize both systems. Therefore, the structure of mucus and HEC gels was analyzed by cryo-SEM imaging of native respiratory mucus.

6.5.3 Cryo-SEM

The results presented here could confirm the findings obtained by the described capillary experiments: Indeed, a pore size approaching the diameter of the penetrating particles of approximately 200 nm can be expected to lie between HEC gel concentrations of 0.5 % to 1 %, as predicted by the Chrmbach and Rodbard model. Furthermore, cryo-SEM images pointed out, that in general, particles do penetrate hydrogels upon the application of external forces, even if the pores are much smaller than the particles.

This fact revealed two considerable features of the mucus hydrogel which may have an impact on particle mobility and penetration in this polymer mesh: pore size distribution in conjunction with the thickness of the polymer scaffold. As mentioned above, comparison of cryo-SEM images of HEC gels with the results presented in section 6.4.2 showed that pore size is not always the limiting factor for penetration. Therefore, considering that particles did not penetrate mucus, one would postulate either a high rigidity of the mucin scaffold which resists any rupture or deformation upon application of external forces so that particles are indeed captured in the smaller pores (if existing) or strong adhesive interactions between particles and mucus. The observation of the thick polymer scaffold, a very heterogeneous pore size distribution in mucus (which is in accordance with recent

findings for cervical mucus (Lai, Wang et al., 2010)) and the fact that mucoinert PEGylated particles did not show better penetration into mucus, suggests the former to be the dominant mechanism here. The very thick polymer scaffold in mucus (figure 25) may be composed of thick mucin bundles as suggested by an earlier study (Lai, Wang et al., 2010). The consequences of such rigid and thick polymer structure were further assessed in section 6.4.4. In summary, to describe mobility of particles in mucus, both size sieving effects as well as interaction filtering have to be considered - however only in addition to the evaluation of mechanical properties of the polymer scaffold: The results described above demonstrate that the key feature of mucus is its highly rigid structure in conjunction with the observed heterogeneous pore size distribution of very small but also large pores. Assessment of the first point was performed with optical tweezers as advanced tool to study active microrheology in a non-invasive way.

6.5.4 Optical Tweezers

The broad distribution of pore size in mucus (section 6.4.3) may be the reason for a broad statistical spread of its rheological behavior (figures 26, 28, 29). Particles located in smaller pores seem less mobile than particles located in large pores. In any case, however, particles in mucus could not be translocated by trapping and the deflection of optical traps.

Contrary, no comparably large pores exist within HEC gels. This resulted in a much more homogeneous material response. Together with relatively small pore sizes, the elastic as well as the viscous modulus measured by passive tracking experiments in the setup of optical tweezers showed comparable or even bigger values for HEC gels depending on the excitation frequency. Active deflection of the beads was, however, possible for HEC gels.

Thus, while in mucus the MSD may pretend a large spread in particle mobility (with few quite mobile particles), macroscopic capillary penetration experiments (see corresponding section) and active particle deflection by optical traps challenged this result: In HEC gels, particles could be driven actively through the fluid despite the MSD indicating a more homogeneous but yet a similar confinement as in mucus. As sketched in figure 31, particles in HEC gels are probably dispersed in dense gels of small pore sizes.

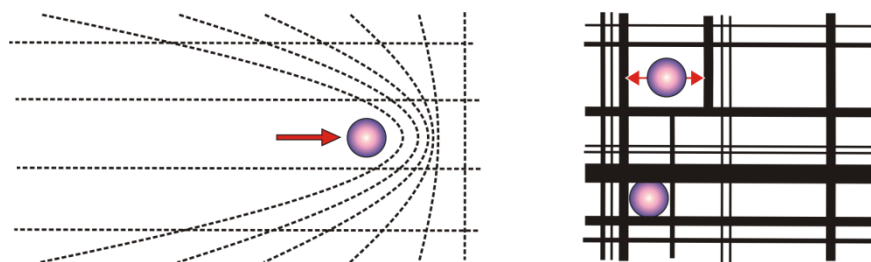


Figure 31: Particles in HEC hydrogels can be displaced easily by external force fields due to a polymer mesh which can be deformed or even ruptured (left). In mucus, particle mobility is determined mainly by the size of the respective pore the particle is located in. The rigidity of the mucin scaffold, however, impedes displacement of the particle out of such voids (right).

The key feature here is that contrary to mucus, upon actively displacing a bead, the polymer scaffold of HEC gels may be deformed or even ruptured. In mucus, the mobility of particles depends on the local pore size as the encounter of the bead with the wall of the respective pore limits its mobility: Due to the polymer scaffold rigidity the beads cannot be moved over larger distances. Therefore, the investigation of the microrheology by passive particle tracking (measurement of MSD and further processing to calculate rheological parameters) must not remain the sole method to extrapolate to particle translocations over larger distances. This is particularly true for tracking experiments with very short correlation times. It was shown in this study that a setup of optical tweezers is a reliable tool not only to determine the microrheology of a material but also auxiliary parameters such as pore rigidity and size on the micron scale.

6.6 Conclusion

A combination of novel tools such as cryo-SEM, capillary penetration or optical tweezers was applied to assess particle mobility in and penetration through mucus and model hydrogels on various length scales. It could be shown that the thorough assessment of particle penetration through mucus cannot be described solely by methods focusing on only one scale, be it micro-, meso-, or macroscopic behavior. It was demonstrated that neither adhesive or non-adhesive particle-mucus interactions, nor the pore size of the hydrogel alone are sufficient parameters to describe particle mobility in mucus: HEC hydrogels with much smaller pore sizes and comparable elastic and viscous modulus were even shown to be penetrated more easily by magnetic particles than mucus. It was discovered, that this discrepancy may be caused by differences in rigidity of the polymer scaffold which was assessed by optical tweezers and a broad pore size distribution in mucus. The observed differences in particle mobility due to surface chemistry as described in the literature may thus be due to differences in particle adhesion to mucins within larger voids of mucus. Therefore, this study presents the so far missing linkage between microrheology and macroscopical observations regarding particle mobility in mucus.

7. Overall Conclusion and Outlook

The presented work illuminates the fate of inhaled material after encountering the mucus layer as primary and most important non-cellular component of the air-blood barrier of the upper lungs. Here, all main aspects of particle-mucus interactions such as fluid dynamics and physical interactions were taken into account, in particular with respect to mucociliary clearance and particle mobility in mucus.

- The identification of possible, yet unknown parameters affecting mucociliary clearance was one of the major goals of the presented work. As it is displayed in the first section of this study, we could show for the first time to our knowledge that particle fate upon deposition as influenced by mucociliary clearance does not depend on particle properties such as size, shape, charge and surface chemistry of the particles under investigation. This was demonstrated in an *ex vivo* setup with high relevance to the *in vivo* situation. A lack of relative velocity between transported particles and their surrounding medium, the moving mucus blanket, was concluded to be the reason for the observed independency on individual particle properties. With mucociliary clearance velocity giving indirect evidence for particle penetration through mucus, it was hypothesized that particles do not sediment upon deposition on an intact and compact mucus layer. Therefore, a possible small fraction of particles translocating to the epithelium was considered to take advantage of turbulent mucus flow or of heterogeneities in the mucus mesh such as larger voids or poorly covered patches of the epithelium. This hypothesis was the foundation of the work presented in the second section.
- Here, mucus fluid dynamics was assessed by analytical and numerical methods. It could be confirmed that, indeed, nanoparticles being deposited onto the mucus blanket do not sediment or translocate into mucus due to impaction or gravitation. This behavior leads to an only negligible time span where a relative velocity between mucus and the particles still exists which is however a precondition to observe differences in mucociliary clearance. Again, this approach is unique in current research and contributed to clarify the fate of particles deposited on the mucus blanket. The remaining mechanism potentially susceptible to particle properties and thus being able to cause differences in translocation through the mucus blanket is translocation due to turbulent mucus flow, heterogeneous surface coverage or collision and spreading of mucus flakes. This was proven feasible in a computational approach. Particle diffusion as further mechanism for particle

translocation however, so far only considered in a simplified approach in the described experiments and calculations, is highly dependent on mucus structure, rheology and particle-mucus interactions. Therefore, these parameters needed to be additionally investigated as it is shown in the third experimental section.

- As specified in the aim of the thesis, the parameters mentioned above were hypothesized to be crucial factors for particle mobility in mucus. Here, the presented unique approach combining macro- and microscopic investigation of particle mobility, mucopenetration, mucus structure and rheology revealed several key features of mucus inhibiting particle mobility on mesoscopic scales: Contrary to chitosan coated particles, PEGylated particles were shown not to adhere to mucin fibers. Despite of these, indeed, large differences in adhesive particle-mucus interactions, particle penetration through mucus filled capillaries could surprisingly not be observed for any particle type, resisting the applied external magnetic field. Cryo-SEM analysis of the structure of mucus and HEC gels lead to the following conclusion: Mucus heterogeneity in pore size and the thick, possibly rigid, polymer scaffold may be the reason for large differences in particle mobility on the microscopic scale but impede translocation over larger distances. These postulated points were confirmed by experiments involving optical tweezers where active deflection of trapped beads revealed that, indeed, even high forces cannot overcome the restricting rigid walls of the pores inside mucus.

In the future, possibilities to overcome this rigid mucus barrier on the individual particle level need to be assessed. Here, previous works as presented by Kuhn et al. (Kuhn, Hallahan et al., 2006) proposed effective mechanisms such as the degradation of the surrounding polymer mesh by enzymes bound to the particles' surface as highly potential delivery system for mucosal surfaces. Furthermore the indirect approach of using particles adhesive to the epithelial cells and thus taking advantage of patches of the epithelium which are poorly covered with mucus, seems to be suitable to increase the particle concentration in the vicinity of the epithelium.

8. List of Figures

Figure 1.....	- 5 -
Figure 2.....	- 8 -
Figure 3.....	- 9 -
Figure 4.....	- 10 -
Figure 5.....	- 14 -
Figure 6.....	- 14 -
Figure 7.....	- 20 -
Figure 8.....	- 22 -
Figure 9.....	- 25 -
Figure 10.....	- 26 -
Figure 11.....	- 35 -
Figure 12.....	- 36 -
Figure 13.....	- 41 -
Figure 14.....	- 43 -
Figure 15.....	- 45 -
Figure 16.....	- 52 -
Figure 17.....	- 53 -
Figure 18.....	- 54 -
Figure 19.....	- 59 -
Figure 20.....	- 60 -
Figure 21.....	- 61 -
Figure 22.....	- 62 -
Figure 23.....	- 63 -
Figure 24.....	- 63 -
Figure 25.....	- 64 -
Figure 26.....	- 65 -
Figure 27.....	- 65 -
Figure 28.....	- 67 -
Figure 29.....	- 67 -
Figure 30.....	- 68 -
Figure 31.....	- 72 -

9. List of Abbreviations

API	Active Pharmaceutical Ingredient
AFM	Atomic Force Microscopy
CF	Cystic Fibrosis
CFD	Computational Fluid Dynamics
COPD	Chronic Obstructive Pulmonary Disease
CV	Coefficient of Variation
Cryo-SEM	Cryo Scanning Electron Microscopy
DAPI	4',6-diamidino-2-phenylindole
DLS	Dynamic Light Scattering
DPM	Discrete Phase Model
e.g.	exempli gratia
ECT	Embryonic Chicken Trachea
FITC	fluorescein isothiocyanate
FPM	Finite-Pointset Method
FWHM	Full Width at Half Maximum
HEC	Hydroxyethylcellulose
i.e.	id est
MSD	Mean Squared Displacement
NTA	Nanoparticle Tracking Analysis
PAA	Polyacrylic Acid
PC	Phosphatidylcholine
PCL	Periciliary Layer
PEG	Polyethyleneglycol
PEI	Polyethylenimin
PMMA	Polymethacrylate
PS	Polystyrene
PSD	Power Spectral Density
SAM	Self-Assembled Monolayer
SD	Standard Deviation
VOF	Volume-Of-Fluid

References

Addas, K. M., Schmidt, C. F., et al. (2004). *Microrheology of solutions of semiflexible biopolymer filaments using laser tweezers interferometry*. Phys Rev E Stat Nonlin Soft Matter Phys 70(2 Pt 1): 021503.

Andrews, G. P., Lavery, T. P., et al. (2009). *Mucoadhesive polymeric platforms for controlled drug delivery*. Eur J Pharm Biopharm 71(3): 505-518.

Antunes, M. B. and Cohen, N. A. (2007). *Mucociliary clearance--a critical upper airway host defense mechanism and methods of assessment*. Curr Opin Allergy Clin Immunol 7(1): 5-10.

Bailey, M. M. and Berkland, C. J. (2009). *Nanoparticle formulations in pulmonary drug delivery*. Med. Res. Rev. 29(1): 196-212.

Barton, C. and Raynor, S. (1967). *Analytical investigation of cilia induced mucous flow*. Bull Math Biophys 29(3): 419-428.

Bastacky, J., Lee, C. Y., et al. (1995). *Alveolar lining layer is thin and continuous: low-temperature scanning electron microscopy of rat lung*. J Appl Physiol 79(5): 1615-1628.

Bennett, W. D. (2002). *Effect of beta-adrenergic agonists on mucociliary clearance*. J Allergy Clin Immunol 110(6 Suppl): S291-297.

Boucher, R. C. (2007). *Airway surface dehydration in cystic fibrosis: pathogenesis and therapy*. Annu Rev Med 58: 157-170.

- Button, B. and Boucher, R. C.** (2008). *Role of mechanical stress in regulating airway surface hydration and mucus clearance rates*. *Respir Physiol Neurobiol* 163(1-3): 189-201.
- Champion, J. A., Katare, Y. K., et al.** (2007). *Making polymeric micro- and nanoparticles of complex shapes*. *Proc Natl Acad Sci U S A* 104(29): 11901-11904.
- Cheezum, M. K., Walker, W. F., et al.** (2001). *Quantitative comparison of algorithms for tracking single fluorescent particles*. *Biophys J* 81(4): 2378-2388.
- Chrambach, A. and Rodbard, D.** (1971). *Polyacrylamide gel electrophoresis*. *Science* 172(3982): 440-451.
- Cinti, C., Taranta, M., et al.** (2011). *Newly engineered magnetic erythrocytes for sustained and targeted delivery of anti-cancer therapeutic compounds*. *PLoS One* 6(2): e17132.
- Cone, R. A.** (2009). *Barrier properties of mucus*. *Adv Drug Deliv Rev* 61(2): 75-85.
- Crater, J. S. and Carrier, R. L.** (2010). *Barrier properties of gastrointestinal mucus to nanoparticle transport*. *Macromol Biosci* 10(12): 1473-1483.
- Dawson, M., Wirtz, D., et al.** (2003). *Enhanced viscoelasticity of human cystic fibrotic sputum correlates with increasing microheterogeneity in particle transport*. *J Biol Chem* 278(50): 50393-50401.
- Donaldson, S. H., Corcoran, T. E., et al.** (2007). *Mucociliary clearance as an outcome measure for cystic fibrosis clinical research*. *Proc Am Thorac Soc* 4(4): 399-405.

Fiegel, J., Jin, F., et al. (2005). *Wetting of a particle in a thin film*. J Colloid Interface Sci 291(2): 507-514.

Filipe, V., Hawe, A., et al. (2010). *Critical evaluation of Nanoparticle Tracking Analysis (NTA) by NanoSight for the measurement of nanoparticles and protein aggregates*. Pharm Res 27(5): 796-810.

Fischer, K. E., Aleman, B. J., et al. (2009). *Biomimetic nanowire coatings for next generation adhesive drug delivery systems*. Nano Lett 9(2): 716-720.

Florey, H. W. (1962). *The secretion and function of intestinal mucus*. Gastroenterology 43: 326-329.

Fulford, G. R. and Blake, J. R. (1986). *Muco-ciliary transport in the lung*. J Theor Biol 121(4): 381-402.

Gastaldi, A. C., Jardim, J. R., et al. (2000). *The influence of temperature and length of time of storage of frog mucus samples*. Biorheology 37(3): 203-211.

Gehr, P., Green, F. H., et al. (1996). *Airway surfactant, a primary defense barrier: mechanical and immunological aspects*. J Aerosol Med 9(2): 163-181.

Gehr, P., Im Hof, V., et al. (2000). *The mucociliary system of the lung--role of surfactants*. Schweiz Med Wochenschr 130(19): 691-698.

Geiser, M., Cruz-Orive, L. M., et al. (1990). *Assessment of particle retention and clearance in the intrapulmonary conducting airways of hamster lungs with the fractionator*. J Microsc 160(Pt 1): 75-88.

Geiser, M., Gerber, P., et al. (2000). *Retention of Teflon particles in hamster lungs: a stereological study.* J Aerosol Med 13(1): 43-55.

Geiser, M., Im Hof, V., et al. (1997). *Ultrastructure of the aqueous lining layer in hamster airways: is there a two-phase system?* Microsc Res Tech 36(5): 428-437.

Geiser, M. and Kreyling, W. G. (2010). *Deposition and biokinetics of inhaled nanoparticles.* Part Fibre Toxicol 7: 2.

Geiser, M., Serra, A. L., et al. (1995). *Efficiency of airway macrophage recovery by bronchoalveolar lavage in hamsters: a stereological approach.* Eur Respir J 8(10): 1712-1718.

Gfeller, K. Y., Nugaeva, N., et al. (2005). *Rapid biosensor for detection of antibiotic-selective growth of Escherichia coli.* Appl Environ Microbiol 71(5): 2626-2631.

Henning, A., Schneider, M., et al. (2008). *Embryonic chicken trachea as a new in vitro model for the investigation of mucociliary particle clearance in the airways.* AAPS PharmSciTech 9(2): 521-527.

Henning, A., Schneider, M., et al. (2010). *Influence of particle size and material properties on mucociliary clearance from the airways.* Journal of Aerosol Medicine and Pulmonary Drug Delivery 23(4): 233-241.

Hirt, C. W. and Nichols, B. D. (1981). *Volume of fluid (VOF) method for the dynamics of free boundaries.* J Comput Phys 39(1): 201-225.

Hofmann, W. and Asgharian, B. (2003). *The effect of lung structure on mucociliary clearance and particle retention in human and rat lungs.* Toxicol Sci 73(2): 448-456.

- Im Hof, V., Gehr, P., et al.** (1997). *In vivo determination of surface tension in the horse trachea and in vitro model studies*. Respir Physiol 109(1): 81-93.
- Iravani, J. and Melville, G. N.** (1976). *Mucociliary function in the respiratory tract as influenced by physicochemical factors*. Pharmacol Ther B 2(3): 471-492.
- Khanvilkar, K., Donovan, M. D., et al.** (2001). *Drug transfer through mucus*. Adv Drug Deliv Rev 48(2-3): 173-193.
- King, M.** (2006). *Physiology of mucus clearance*. Paediatr Respir Rev 7 Suppl 1: S212-214.
- Koch, A. M., Reynolds, F., et al.** (2005). *Transport of surface-modified nanoparticles through cell monolayers*. Chembiochem 6(2): 337-345.
- Kreuter, J.** (1991). *Nanoparticle-based drug delivery systems*. J Control Release 16(1-2): 169-176.
- Kuhn, S. J., Hallahan, D. E., et al.** (2006). *Characterization of superparamagnetic nanoparticle interactions with extracellular matrix in an in vitro system*. Ann Biomed Eng 34(1): 51-58.
- Lai, S. K., O'Hanlon, D. E., et al.** (2007). *Rapid transport of large polymeric nanoparticles in fresh undiluted human mucus*. Proc Natl Acad Sci U S A 104(5): 1482-1487.
- Lai, S. K., Wang, Y. Y., et al.** (2009). *Mucus-penetrating nanoparticles for drug and gene delivery to mucosal tissues*. Adv Drug Deliv Rev 61(2): 158-171.

- Lai, S. K., Wang, Y. Y., et al.** (2010). *Nanoparticles reveal that human cervicovaginal mucus is riddled with pores larger than viruses*. Proc Natl Acad Sci U S A 107(2): 598-603.
- Lai, S. K., Wang, Y. Y., et al.** (2009). *Micro- and macrorheology of mucus*. Adv Drug Deliv Rev 61(2): 86-100.
- Landau, L. D. and Lifshitz, E. M.** (1966). *In course of theoretical physics: statistical physics part I*. 5: 371-389.
- Lieleg, O. and Ribbeck, K.** (2011). *Biological hydrogels as selective diffusion barriers*. Trends Cell Biol 21(9): 543-551.
- Livraghi, A. and Randell, S. H.** (2007). *Cystic fibrosis and other respiratory diseases of impaired mucus clearance*. Toxicol Pathol 35(1): 116-129.
- Macierzanka, A., Rigby, N. M., et al.** (2011). *Adsorption of bile salts to particles allows penetration of intestinal mucus*. Soft Matter 7: 8077.
- Matsui, H., Randell, S. H., et al.** (1998). *Coordinated clearance of periciliary liquid and mucus from airway surfaces*. J Clin Invest 102(6): 1125-1131.
- Moller, W., Felten, K., et al.** (2008). *Deposition, retention, and translocation of ultrafine particles from the central airways and lung periphery*. Am J Respir Crit Care Med 177(4): 426-432.
- Mura, S., Hillaireau, H., et al.** (2011). *Biodegradable nanoparticles meet the bronchial airway barrier: how surface properties affect their interaction with mucus and epithelial cells*. Biomacromolecules 12(11): 4136-4143.

- Oberdorster, G., Oberdorster, E., et al.** (2005). *Nanotoxicology: an emerging discipline evolving from studies of ultrafine particles*. Environ Health Perspect 113(7): 823-839.
- Olmsted, S. S., Padgett, J. L., et al.** (2001). *Diffusion of macromolecules and virus-like particles in human cervical mucus*. Biophys J 81(4): 1930-1937.
- Patton, J. S. and Byron, P. R.** (2007). *Inhaling medicines: delivering drugs to the body through the lungs*. Nat Rev Drug Discov 6(1): 67-74.
- Peppas, N. A. and Huang, Y.** (2004). *Nanoscale technology of mucoadhesive interactions*. Adv Drug Deliv Rev 56(11): 1675-1687.
- Powell, R. L., Aharonson, E. F., et al.** (1974). *Rheological behavior of normal tracheobronchial mucus of canines*. J Appl Physiol 37(3): 447-451.
- Randell, S. H. and Boucher, R. C.** (2006). *Effective mucus clearance is essential for respiratory health*. Am J Respir Cell Mol Biol 35(1): 20-28.
- Sanders, N., Rudolph, C., et al.** (2009). *Extracellular barriers in respiratory gene therapy*. Adv Drug Deliv Rev 61(2): 115-127.
- Sanders, N. N., De Smedt, S. C., et al.** (2003). *Mobility and stability of gene complexes in biogels*. J Control Release 87(1-3): 117-129.
- Sanders, N. N., De Smedt, S. C., et al.** (2000). *Cystic fibrosis sputum: a barrier to the transport of nanospheres*. Am J Respir Crit Care Med 162(5): 1905-1911.
- Sarbolouki, M. N., Mahnam, K., et al.** (2004). *Determination of pore/protein size via electrophoresis and slit sieve model*. Electrophoresis 25(17): 2907-2911.

- Scheuch, G., Kohlhaeufel, M. J., et al.** (2006). *Clinical perspectives on pulmonary systemic and macromolecular delivery*. Adv Drug Deliv Rev 58(9-10): 996-1008.
- Schnurr, B., Gittes, F., et al.** (1997). *Determining microscopic viscoelasticity in flexible and semiflexible polymer networks from thermal fluctuations* Macromolecules 30: 7781-7792.
- Schurch, S., Gehr, P., et al.** (1990). *Surfactant displaces particles toward the epithelium in airways and alveoli*. Respir Physiol 80(1): 17-32.
- Schürch, S., Gehr, P., et al.** (1990). *Surfactant displaces particles toward the epithelium in airways and alveoli*. Respir Physiol 80(1): 17-32.
- Shannon, C. E.** (1949). *Communication in the presence of noise*. Proceedings of the IRE 37: 10-21.
- Simmons, R. M., Finer, J. T., et al.** (1996). *Quantitative measurements of force and displacement using an optical trap*. Biophys J 70(4): 1813-1822.
- Sims, D. E. and Horne, M. M.** (1997). *Heterogeneity of the composition and thickness of tracheal mucus in rats*. Am J Physiol 273(5 Pt 1): L1036-1041.
- Smart, J. D.** (2005). *The basics and underlying mechanisms of mucoadhesion*. Adv Drug Deliv Rev 57(11): 1556-1568.
- Smith, D. J., Gaffney, E. A., et al.** (2007). *A viscoelastic traction layer model of mucociliary transport*. Bull Math Biol 69(1): 289-327.

- Smith, D. J., Gaffney, E. A., et al.** (2008). *Modelling mucociliary clearance*. *Respir Physiol Neurobiol* 163(1-3): 178-188.
- Tarran, R., Trout, L., et al.** (2006). *Soluble mediators, not cilia, determine airway surface liquid volume in normal and cystic fibrosis superficial airway epithelia*. *J Gen Physiol* 127(5): 591-604.
- Thornton, D. J. and Sheehan, J. K.** (2004). *From mucins to mucus: toward a more coherent understanding of this essential barrier*. *Proc Am Thorac Soc* 1(1): 54-61.
- Tiwari, S. and Kuhnert, J.** (2002). *Finite pointset method based on the projection method for simulations of the incompressible Navier-Stokes equations*. Springer LNCSE: Meshfree methods for Partial Differential Equations 26.
- Tiwari, S. A., Hietel, D., et al.** (2006). *Meshfree method for simulations of interactions between fluids and flexible structures, lecture notes in computational science and engineering*. Meshfree Methods for Partial Differential Equations III: 249 - 264.
- Tseng, P., Di Carlo, D., et al.** (2009). *Rapid and dynamic intracellular patterning of cell-internalized magnetic fluorescent nanoparticles*. *Nano Lett* 9(8): 3053-3059.
- Valentine, M. T., Perlman, Z. E., et al.** (2004). *Colloid surface chemistry critically affects multiple particle tracking measurements of biomaterials*. *Biophys J* 86(6): 4004-4014.
- van As, A. and Webster, I.** (1972). *The organization of ciliary activity and mucus transport in pulmonary airways*. *S Afr Med J* 46(13): 347-350.
- Verdugo, P.** (1991). *Mucin exocytosis*. *Am Rev Respir Dis* 144(3 Pt 2): S33-37.

Verdugo, P., Deyrup-Olsen, I., et al. (1987). *Molecular mechanism of mucin secretion: I. The role of intragranular charge shielding.* J Dent Res 66(2): 506-508.

Widdicombe, J. H. (2002). *Regulation of the depth and composition of airway surface liquid.* J Anat 201(4): 313-318.

Yoncheva, K., Lizarraga, E., et al. (2005). *Pegylated nanoparticles based on poly(methyl vinyl ether-co-maleic anhydride): preparation and evaluation of their bioadhesive properties.* Eur J Pharm Sci 24(5): 411-419.

Ziehl, A., Bammert, J., et al. (2009). *Direct measurement of shear-induced cross-correlations of Brownian motion.* Phys Rev Lett 103(23): 230602.

Curriculum Vitae

PERSONAL

Date of birth: January 19th, 1984 in Saarbruecken

Marital Status: married

EDUCATION

09/2009 – 05/2012 Doctoral thesis at *Saarland University*, AG Lehr with the title: “*The Role of Fluid Dynamics, Microstructure and Mucociliary Clearance in the Micro- and Macroscopic Barrier Properties of Pulmonary Mucus*”

10/2008 – 08/2009 Diploma thesis at the *Technical University Kaiserslautern*, AG Ziegler with the title: “*Rasterkraftmikroskopische Charakterisierung von Biofilmen auf Dentalmaterialien*“, granting of the diploma in biophysics

10/2004 – 10/2008 Undergraduate studies of biophysics at the *Technical University Kaiserslautern*

03/2003 Graduation at the „*Staatl. Gymnasium Hermeskeil*“

1994 – 2003 *Staatl. Gymnasium Hermeskeil*

AWARDS

03/2011 INTERNATIONAL SOCIETY FOR AEROSOLS IN MEDICINE
Student Research Award 2011, third prize

ZIVILDIENT

05/2003 – 05/2004 Zivilidienst at the *Schule und Internat für Blinde und Gehörlose*,
Lebach

INTERNSHIPS

08/2008 Internship at the *Fraunhofer Institut for Biomedical Engineering*
(*IBMT*), St. Ingbert

05/2003 Internship at the *Landesamt für Gesundheit und Verbraucherschutz*,
Saarbruecken

INTERNATIONAL EXPERIENCE

06/2004 – 08/2004 Volunteering at the farm *Sidri-Vellir*, Iceland

08/2000 – 07/2001 Study at the *Worcester Academy*, Worcester, USA

List of Publications

Scientific Publications

Kirch, J., Guenther, M., et al. (2012). *Mucociliary clearance of micro- and nanoparticles is independent of size, shape and charge—an ex vivo and in silico approach.* J Control Release 159(1): 128-134

Kirch, J., Guenther, M., et al. (2012). *Computational fluid dynamics of nanoparticle disposition in the airways: mucus interactions and mucociliary Clearance.* Comput Visual Sci: accepted

Kirch, J., Schneider, A., et al. (2012). *Optical tweezers reveal relationship between microrheology and particle penetration of pulmonary mucus.* submitted for publication

Ruge, C. A., Kirch, J., et al. (2011). *Uptake of nanoparticles by alveolar macrophages is triggered by surfactant protein A.* Nanomedicine: NBM 7: 690-693

Kirch, J., Ruge, C. A., et al. (2012). *Nanostructures overcoming the pulmonary barrier: Physiological considerations and mechanistic issues.* RSC drug discovery series: Nanostructured biomaterials for overcoming biological barriers: Book Chapter

Pfeifer, C., Hasenpusch, G., et al. (2011). *Dry powder aerosols of polyethylenimine (PEI)-based gene vectors mediate efficient gene delivery to the lung.* J Control Release 154 (1): 69-76

Poster & Talks

Kirch, J. Schneider, M., et al. (2011). *computational fluid dynamics of nanoparticle deposition in mucus and mucociliary clearance*. ISAM Congress, Rotterdam (NED): Poster

Kirch, J., Guenther, M., et al. (2011). *Computational fluid dynamics of nanoparticle deposition in the lung and mucociliary clearance*. Modeling Biological Membranes, Frankfurt (D): Talk

Kirch, J. Schneider, A., et al. (2010). *New methods and models to investigate interactions between nanoparticles and mucus*. Biological Barriers, Saarbruecken (D): Poster

Kirch, J. Schneider, M., et al. (2010). *Mucociliary clearance of nanoparticles - computer-assisted image analysis*. Aerosol Seminar, Marburg (D): Poster

Kirch, J. Schneider, M., et al. (2010). *Improved particle tracking in mucociliary clearance experiments by simultaneous application of differently labelled particles*. PSWC World Congress, New Orleans (USA): Poster

Mueller, C., Wald, J., et al. (2010). *Bioadhesion on surfaces in the oral cavity – a combined surface analytical approach*. ESB, 23rd European Conference on Biomaterials, Tampere (Finnland): Poster

Huber, C., Kirch, J., et al. (2010). *Untersuchungen der Protein-Protein-Wechselwirkung in dentalen Biofilmen*. 16. Arbeitstagung Angewandte Oberflächenanalytik (AOFA), Kaiserslautern (D): Poster

Mueller, C., Lueders, A., et al. (2009). *Initial bioadhesion on surfaces in the oral cavity investigated by different surface science methods*. Euro AFM Forum, Garching (D): Poster

Kirch, J., Mueller, C., et al. (2009). *Protein-protein interaction on dental surfaces*. Euro AFM Forum, Garching (D): Talk

Kirch, J., Mueller, C., et al. (2009). *Protein-protein interactions on dental surfaces studied by scanning force spectroscopy (SFS)*. SPM and Organic Materials XVII, Bremen (D): Poster

Kirch, J., Mueller, C., et al. (2009). *Protein-protein interactions on dental surfaces studied by scanning force spectroscopy (SFS)*. Euro AFM Forum, Garching (D): Poster

Acknowledgements

First of all I would like to thank Prof. Dr. Claus-Michael Lehr who gave me the opportunity to develop not only my scientific skills but also my personality to a great extend. In addition I would like to thank him for his creative advice during the last years and the trust he has put into myself and the way we approached the goal of our research. It has been great to enjoy his passion and determination.

Additionally, I feel deeply grateful towards Prof. Dr. Ulrich Schaefer as my main advisor who contributed to so much of our scientific work and has been delightful to work with throughout my time at Saarland University.

Furthermore, I would especially like to thank Andreas Schneider and Prof. Dr. Marco Guenther which contributed some much to the work presented here and were always open for discussion and new approaches.

To Christian Ruge and Prof. Dr. Marc Schneider for their social and technical support: Thank you very much! Without the both of you the last years would have been much less enjoyable.

In addition, I greatly appreciate the constant advice of Prof. Dr. Ingolf Bernhardt who helped me a lot to improve the results presented here.

I also thank all my colleagues for the brilliant spirit among the Ph.D. students and the amicable atmosphere in the lab! It was great to get to know all of you! Furthermore, a big thank you goes to all our technicians who make our work possible in the first place.

Furthermore, I would like thank the German Research Association for the generous funding of the project.